Consortium for
Electric
Reliability
Technology
Solutions

Real-Time
Voltage Security
Assessment
(RTVSA)

RTVSA REPORT

ON

ALGORITHMS & FRAMEWORK

Prepared For
California Independent System Operator (CA ISO)

Prepared By
Consortium for Electric Reliability Technology Solutions (CERTS)

Funded By:
California Public Interest Energy Research
Transmission Research Program

Revised June 9, 2008

CERTS
CONSORTIUM FOR ELECTRIC RELIABILITY TECHNOLOGY SOLUTIONS

PREPARED FOR:

California Independent System Operator

PREPARED BY:

Electric Power Group
Manu Parashar, Ph.D. - Principal Investigator
Abhijeet Agarwal - Investigator

Pacific Northwest National Laboratory
Yuri Makarov, Ph.D. - Principal Consultant

University of Wisconsin, Madison
Ian Dobson, Ph.D. - Consultant

DATE:

Revised June 2008

Acknowledgements

Electric **P**ower **G**roup

TABLE OF CONTENTS

✳ **E**lectric **P**ower **G**roup

LIST OF FIGURES

Electric Power Group

1. Introduction and Background

Over the past 40 years, more than 30 major blackouts worldwide were related to voltage instability and collapse. Among them, at least 13 voltage-related blackouts happened in the United States, including two major blackouts in the Western Interconnection in 1996 and a wide-scale blackout in the Eastern Interconnection in 2003. Several times, the blackout investigation teams indicated the need for on-line power flow and stability tools and indicators for voltage performance system-wide in a real-time. These recommendations are not yet completely met by the majority of US power system control centers. The gap between the core power system voltage and reliability assessment needs and the actual availability and use of the voltage security analysis tools was a motivation to come forward with this project. The project aims to develop state-of-the-art methodologies, prototypes and technical specifications for the Real-Time Voltage Security Assessment (RTVSA) tools. These specifications can be later used by selected Vendors to develop industrial-grade applications for California Independent System Operator (CA ISO), other California Control Area Operators, and utilities in California.

Currently CA ISO's real time operations do not have a real-time dispatcher's Voltage Security Assessment tool and corresponding wide-area visuals to effectively manage the voltage and VAR resources on the transmission system and to identify the following:

- Voltage security margin calculation
- Worst-case contingencies leading to voltage collapse
- Abnormal reductions of nodal voltages
- Contingency ranks according to a severity index for system problems
- System conditions with insufficient stability margin
- Weakest elements within the grid
- Controls to increase the available stability margin and avoid instability

The objectives of this report are to present a comprehensive survey of algorithms available worldwide for the purpose of performing voltage security assessment, make recommendations on the most appropriate techniques, and describe a framework along with the algorithms that have been included in the prototype RTVSA tool.

The California Energy Commission (CEC), with input from CA ISO, requested an initiative to explore better avenues to optimize utilization of the existing transmission. As the first step to achieve this objective, Consortium for Electric Reliability Technology Solutions (CERTS)/Electric Power Group (EPG) formulated a survey to reach out to experts in this field for comments, information, suggestions, and recommendations. The choice of the PSERC (Power Systems Engineering Research Center) engine as a basis for building the VSA prototype was motivated by the results of the survey (described in Section 4). The algorithmic details can be found in Section 5.

2. Existing VSA Methods

Voltage instability and voltage collapse are complicated phenomena that depend on the interactions of multiple system components and power flow parameters including generators, excitation control and over excitation protection, voltage regulators, reactive power sources, components of the transmission and distribution system, such as switching capacitors, under load tap changers, static VAR compensators reaching reactive power limits and loads, such as induction motors, thermostats, manual activities that respond to the decaying voltage and attempt to restore the load to its original demand in spite of decaying voltage and other static and dynamic load characteristics. It is necessary to distinguish large-disturbance voltage stability, vulnerability to cascading events, and small disturbance voltage stability.

▪ *Large-disturbance voltage stability* deals with the system ability to maintain voltages after such disturbances as generation trips, load loss, and system faults. It is analyzed by modeling long-term system dynamics. Large-disturbance voltage stability is analyzed by solving a set of nonlinear differential or algebraic equations (time domain simulations or numerical solution) [1], [33]. The system is considered voltage stable if its post-transient voltage magnitudes remain limited by certain pre-established reliability limits (5-10% depending on the severity of disturbance).

▪ *Cascading voltage collapse* can be caused by a sequence of power system changes, as for example, when groups of induction motors stall in succession or when a series of generator reactive power limits are reached in succession. For cascading events, the NERC (North America Electric Reliability Council) and WECC (Western Electricity Coordination Council) reliability criteria require the grid planners to evaluate their risk and consequences [27]. There are just a few techniques developed to assist in understanding or simulating cascading collapses - see [42] for example. The main approach seems to be working out the sequence of events of each individual cascading outage with assistance from simulations. The more advanced time domain simulations can reproduce cascading outages. [31]

▪ *Small-disturbance stability* is concerned with the ability of the system to control voltages following small perturbations or gradual change of parameters such as system load. This type of steady state stability is analyzed by linearizing nonlinear differential equations at a given operating point [1]. Because of the fact that linear differential equations can be solved analytically, there is no need to solve them numerically. There are many methods to check stability of the linearized system without solving it, that is, by analyzing the matrix of its coefficients J (small-signal stability matrix or system Jacobian matrix[1]). The most commonly used approach here involves computing the so-called eigenanalysis of matrix J [1]. The system is asymptotically stable (has positive damping) if all eigenvalues have negative real parts (are located on the left hand side of the complex plane). It is unstable otherwise (has negative damping). Eigenvalues λ are solutions of the characteristic equation $\det(J - \lambda I) = 0$, where I is the identity matrix. Alternatively, the eigenvalue problem can be rewritten as follows: $(J - \lambda I)R = 0$ or $(J^t - \lambda I)L = 0$, where nonzero vectors R and L are *the right and left eigenvectors*, and t is the symbol of matrix transposition.

The WECC Voltage Stability criterion mandates P-V and V-Q studies as the main approaches to analyze voltage stability margins [24].

P-V plots represent the load vs. the voltage of a selected bus. The load is defined as the bus load or the total load in an area or the system. P-V curves are calculated using the power flow solutions by step-by-step increasing the loads. The "nose point" of the curve corresponds to the maximum power which can be delivered to the load. The bus voltage at this point is the critical voltage. If the voltage of one particular bus approaches the nose point faster compared to the other buses, it is assumed that the system voltage stability margin is limited by this bus.

V-Q plots represent the bus voltage vs. reactive power of the same bus. To obtain the curve, a particular bus is assumed to be a voltage controlled bus. A series of power flow simulations are performed for

---

[1] The Jacobian matrix of a set of *n* equations in *n* variables is an *n* × *n* matrix of partial derivatives whose entries are the derivatives of each equation with respect to each variable.

various values of the bus voltage and the corresponding needed reactive injection. The V-Q curves are obtained by plotting the reactive power injection versus the voltage.

V-Q sensitivity analysis is conducted by linearizing the power flow problem and assuming that the active power injections are constant. The linearized system is reduced by eliminating voltage angle increments, and the resulting expression links voltage increments with the reactive power increments. The diagonal elements of the inverse *reduced Jacobian matrix* are sensitivities of the nodal voltages with respect to reactive power injections at the same buses. Large sensitivity indicated reduced stability margin. Negative sensitivity indicates instability.

Q-V modal analysis is based on the analysis of eigenvalues of the reduced Jacobian matrix. The magnitude of the eigenvalues gives the relative measure of the proximity to instability. When the system reaches instability, the modal analysis is helpful in identifying the voltage instability areas and elements which participate in each instability mode (eigenvalue).

Bus participation factors determine the buses associated with each stability mode. The size of bus participation factor indicates the effectiveness of remedial actions in stabilizing the corresponding mode. *Branch participation factors* (calculated for each mode) indicate which branches consume the most reactive power in response to an incremental change in reactive load. Generator *participation factors* indicate which generators supply the most reactive power in response to an incremental change in reactive power loading.

There is a huge interest and variety of methods for the voltage stability/security analysis. Universities, R&D organizations, individual developers and some vendors propose dozens of different promising methods and their modifications. At the same time, the industry has accepted just a few of these approaches as standard methods (i.e., the most traditional approaches such as P-V and V-Q simulations, and transient stability time-domain simulations), leaving the rest of the variety as purely experimental or supplementary tools. The degree of interest to the new VSA tools in the industry vary from one place to another, in some instances it is minimal. This is an unfortunate fact having in mind the importance of the voltage stability/security problem, the existing danger of massive voltage collapses in the U.S. power grids, and the lack of applications such as real-time tools actually used by the industry. One of the objectives pursued by this report is to analyze existing methods, and suggest some of them as state-of-the-art real-time VSA technologies for implementing them at the California ISO, other control areas, and utilities.

The first paper related to voltage instability apparently appeared in 1968 [32], [40]. Since then, numerous approaches for voltage stability assessment have been suggested. In this section, we will outline the techniques using the static voltage stability models with the emphasis on the saddle node bifurcations.

2.1. Stressing Algorithms in a Specified Loading Direction

Step-by-step loading: Traditional power flow calculation methods, such as Newton-Raphson method, are not capable of determining the voltage stability boundary point directly and accurately. They diverge before the point of collapse is reached. The idea of the step-by-step loading is to exploit the quadratic convergence of the Newton-Raphson method in the vicinity of a solution. The procedure starts from a balanced power flow by incrementing the nodal power injections in a specified stress direction using some initial step size. If the Newton-Raphson method converges, the increment is repeated. In case of divergence, the step is divided by two, and by doing so, the next solution point is brought closer to the solution already found along the loading direction. The procedure stops when the step size becomes smaller than some specified accuracy. This method allows the use of detailed power system model including an accurate modeling of equipment limits (such as generator capability limits, switching capacitor limits, transformer tap changer limits, and others) and discrete controls (such as transformer and switching capacitor steps). Computational divergence is not the best criterion to determine the point of collapse since it can be caused by different reasons. [46-48][64].

Step-by-step loading with the analysis of a static small-signal stability criterion: In this method, instead or in addition to the power flow divergence criterion, the determinant (or an eigenvalue with the maximum

real part, or the maximum singular value [65], or the distance between closely located power flow solutions [66]) of the small signal stability matrix J is calculated at each loading step. The moment when the determinant of J changes its sign is considered as the saddle node bifurcation point. This approach also helps to determine the small-signal stability boundary points corresponding to the saddle node or Hopf bifurcations if these points are met before the power flow feasibility boundary is reached [46].

Permanent or continuous loading: This technique uses the Matveev's method for solving the power flow problem [49]. It has been shown that the Matveev's numerical method always converges to a solution or to a point where the power flow Jacobian matrix is singular. The permanent loading (or continuous loading) algorithm [50] exploits that characteristic of the method. In this approach, the loading parameter is set large enough to make sure that the power flow problem does not have a solution (the point is outside of the power flow feasibility boundary in the parameter space). Beginning from the operating point, Matveev's method starts to iterate producing the sequence of points. Approaching the boundary, the step size becomes smaller and smaller. Finally, when the step size becomes small enough and the process is stopped in the vicinity of the power flow feasibility boundary. Due to linearization, the final point is not exactly the point, where the stress vector intersects the power flow feasibility boundary. To eliminate this deviation, a modification of the permanent loading procedure is proposed [51], [52]. In this modification, the permanent loading steps play a role of a "predictor". If the iterative process deviates too much from the loading direction, a "corrector" step is performed. Alternatively the permanent loading process is continued to the point of singularity, and only then the "corrector" step is implemented. This approach is one of the most commonly recognized and frequently used techniques in the industry.

Parameter continuation predictor-corrector methods are the most reliable power flow methods capable of reaching the point of collapse on the power flow feasibility boundary. The addition of new variables, called continuation parameters, determines the position of an operating point along some power system stress direction in the parameter space. The predictor step consists of an incremental movement of the power flow point along the state space trajectory, based on the linearization of the model. The corrector step, which follows each predictor step, consists in the elimination of the linearization error by balancing the power flow equations to some close point on the nonlinear trajectory.

Direct methods for finding the PoC in a given direction combine a parametric description of the system stress, based on the specified loading vector in the parameter space and a scalar parameter describing a position of an operating point along the loading trajectory and the power flow singularity condition expressed with the help of the Jacobian matrix multiplied by a nonzero right or the left eigenvector that nullifies the Jacobian matrix at the collapse point. Unlike the power flow problem, this reformulated problem does not become singular at the point of collapse and can produce the bifurcation point very accurately. In principle, the direct method allows finding the bifurcation points without implementing a loading procedure. There is however, a problem of finding the initial guesses of the state variables and the eigenvector that may be resolved by initial loading the system along the stress direction. By doing so, the initial guess of state variables can be obtained. To evaluate the initial guess for the eigenvector, the Lanczos or inverse iteration[2] methods can be applied to calculate the eigenvector corresponding to the minimum real eigenvalue [58]-[63].

Optimization methods are based on maximization of a scalar parameter describing the position of an operating point along the loading trajectory subject to the power flow balance constraints. The maximum point achieved by the approach corresponds to the point of collapse met on the selected stress trajectory. The solution of this constrained optimization problem is determined by the Karush-Khun-Tucker conditions[3] that produce a set of equations similar to the ones used in the direct method in its variant employing the left eigenvector; Lagrangian multipliers[4] of this problem actually is the left eigenvector

---

[2] Recommended algorithms for computing eigenvector and eigenvectors of the Jacobian matrix. A description of the inverse iteration method is also given in Section 5.5. For more information and references see Eric W. Weisstein. "Lanczos Algorithm." From MathWorld-A Wolfram Web Resourcehttp://mathworld.wolfram.com/LanczosAlgorithm.html

[3] The Karush-Khun-Tucker conditions define properties of a constraint optimization problem solution that can be used to find the optimal point without performing an optimization procedure – see Eric W. Weisstein. "Kuhn-Tucker Theorem." From MathWorld-- A Wolfram Web Resource. http://mathworld.wolfram.com/Kuhn-TuckerTheorem.html

[4] Lagrangian multipliers are variables that help to present a constraint optimization problem an unconstraint optimization problem under certain conditions – see Eric W. Weisstein. "Lagrange Multiplier." From MathWorld--A Wolfram Web Resource. http://mathworld.wolfram.com/LagrangeMultiplier.html

nullifying the power flow Jacobian matrix at the point of collapse. The collapse point can be found directly by solving the set of equations, which is very similar to the direct method, or by applying an optimization method such as the *interior point method*[5] or an alternative *AEMPFAST optimization*[6] procedure that is proven to be able to get very close to the point of collapse of concern [56], [67], [68].

Approaches analyzed in this section assume that the system stress directions are known and reflect some typical load and generation patterns. In the market-driven systems, the generator dispatches are based on their energy bids and transmission congestion, and they may be very different from one dispatch interval to another. Therefore several system stress directions may need to be separately or jointly considered.

2.2. Stressing Algorithms in the Most Critical Direction

Methods for finding the PoC (Point-of-Collapse) in the most critical direction employ the same ideas as the direct methods. The difference is that the stress direction in the parameter space is not fixed, and an additional condition requiring that the system stress vector will be a perpendicular vector with respect to the power flow feasibility boundary at the point of collapse is applied. This direction is called the *critical direction* determining the *shortest distance to instability*. The critical direction coincides with the direction of the left eigenvector nullifying the power flow Jacobian at the closest point of collapse [59], [70]-[73], [1].

By applying this approach, one can evaluate the *worst case stress direction* and the corresponding *critical voltage stability margin* for a given operating point in the parameter space. This is, of course, very useful additional information for the VSA purposes. At the same time, there are some potential problems with this technique that need to be addressed in practical calculations:

- The critical loading direction might be unrealistic or unlikely.

- Due to the nonlinear shape of the power flow feasibility boundary, besides the critical directions, some *sub-critical system stresses* with a comparable voltage stability margin might be observed [74]. In this situation, the critical loading direction does not provide a sufficient characterization of the voltage stability margin.

- The sub-critical stress directions correspond to the local minima of the distance to instability metric. By applying the method, it is hard to tell whether the result corresponds to the global or local minimum, what the other directions are and how many of them exist.

Parameter continuation methods for exploring power flow feasibility boundary. The robust predictor-corrector procedure can be successfully applied to explore the entire structure of the power flow feasibility boundary. Points on the solution boundary are described in the same way it is done in the direct method: using the power flow equations together with an equation which forces the power flow Jacobian to be singular. Contours describing the boundary are obtained by freeing two parameters of the system and following these contours [83].

High-order methods to follow the power flow feasibility boundary. The Newton-Raphson method is based on linearization of the power flow equations at each iteration. The high order method is a generalization of the Newton-Raphson method involving nonlinear terms of the Taylor series expansion [84]. It can be also considered as a parameter continuation technique. The method provides reliable solution of nonlinear algebraic problems up to points of singularity; convergence to a singular point if it occurs on the way of the iterative process; almost straight line motion of the iterative process in the space of power flow mismatches; and retention of zero mismatches. Once an initial point on the power flow feasibility boundary is found, further exploring of the boundary can be done by changing the stress vector in the

---

5 The *interior point method* is a linear or nonlinear programming method that achieves optimization by going through the middle of the solid defined by the problem rather than around its surface - see Eric W. Weisstein, "Interior Point Method." From MathWorld-- A Wolfram Web Resource. http://mathworld.wolfram.com/InteriorPointMethod.html

6 The AEMPFAST algorithm is a trade secret of the Optimal Technologies, Inc. The AEMPFAST software was extensively tested and evaluated by the California ISO. More information on the AEMPFAST can be found in [69].

direction of interest and applying the direct method for exploring the boundary. Since the singularity equation J*R is equal to zero at the initial point, the high order method keeps it near zero during the iteration process; this means that the solution point is automatically kept on the power flow feasibility boundary [85]. The advantages of the analyzed techniques are that they do not require repeating the loading process and calculating multiple interior points of the voltage security region many times to reveal parts of the power flow feasibility boundary.

2.3. Approximation Techniques for Security Regions

Hyperplane and quadratic approximations of the security region: One of the important problems that power system analysts and operators face when they use the concept of the power system security region is the problem of description of the security region's boundary. The simple tabular description is not adequate to the purposes of visualization and practical use by system operators and in the automated VSA systems. There is a need of an *analytical description* and/or *approximation* of the boundary. The analytical description usually means the use of linear or nonlinear inequalities applied to a certain number of *critical parameters* such as power flows, load levels, voltage magnitudes, etc.; if all inequalities are satisfied, the analyzed operating point is considered to be inside the security region; if any of the inequalities is violated, the point is considered to be outside the security region. The approximation means a sort of *interpolation* between the boundary points obtained by any of the methods considered in this section. It can be used as a part of the analytical boundary description (for the automated VSA systems), or separately for the purposes of visualization. The simplest approximation uses *linear inequalities*. The first known use of the approximation ideas was apparently related to the *operating nomograms* – see [78] for more details. The operating nomograms are usually represented visually as piecewise linear contours on a plane of two critical parameters. If three critical parameters are involved, the nomogram is represented by a number of contour lines; each of them corresponds to a certain value of the third parameter. It becomes difficult to visualize a nomogram for four or more critical parameters. The natural extension of the linearized stability nomograms for three or more critical parameters is based on the use of *hyperplanes* - the planes that are defined in the multidimensional parameter space as approximations of the stability boundary. These efforts are described in [80] (voltage stability boundary approximation), [82], [87], [88] (transient/dynamic stability boundary approximation), and other works.

In Russia, in a number of emergency control algorithms, a nonlinear approximation was successfully used to provide an analytical description of the stability boundary [89]. These approaches employ *quadratic inequalities*. The inequalities are applied to the nodal power injections, cutset power flows, and other parameters. The coefficients of these inequalities are pre-calculated offline based on multiple time domain or steady-state stability simulations.

The hyperplane and quadratic approximations have a number of significant advantages:

- They allow to quickly analyze the stability margin in real time

- Due to their formal mathematical nature, they allow to simultaneously consider thermal, voltage stability, transient stability and other constraints within the same framework.

ANN-based techniques [20], [78], [87], [90]-[98]: The idea behind the techniques based on the artificial neural networks is to select a set of critical parameters such as power flows, loads, and generator limits, and then train an ANN on a set of simulation data to estimate the security margin. The ANN model de facto provides an approximation of the stability boundary. The advantages of the ANN models include their ability to accommodate nonlinearities and they are very fast while performing in real time. At the same time, there are difficulties associated with building the training datasets and ANN training.

Pattern recognition methods establish a relationship between some selected parameters and the location of the system operating point with respect to the stability boundary [14,15]. Initially, training sets of stable and unstable operating points are generated, and a space reduction process is applied to reduce the dimensionality of the system model. Then the classifier functions (decision rules) are determined using

the training set. This function is engaged in real time to determine the stability margin of a given contingency [20], [99], [100].

QuickStab algorithm is an alternative method to quickly and approximately evaluate the voltage stability margin in a given loading direction. The idea of this technology was originally developed by Paul Dimo. It includes the voltage stability practical criterion dQ/dV < 0 and Dimo's network nodal equivalents (so called Zero Power Balance Networks or REI[7] equivalents). Dimo's finding is that under certain modeling assumptions the practical stability margin can be expressed as a straightforward formula applied to the nodal equivalents [101], [102].

2.4. Other Techniques

Delta-plane method [113] is a new robust method for finding the power system load flow feasibility boundary on the plane defined by any three vectors of dependent variables (nodal voltages), called the Delta-plane. The method exploits some quadratic and linear properties of the load flow equations (X-ray theorem, [114]) and the power flow Jacobian written in rectangular coordinates. An advantage of the method is that it does not require an iterative solution of nonlinear equations (except the eigenvalue problem). Besides benefits of direct calculation of the power flow feasibility boundary points and visualization, the method is a useful tool for topological studies of power system multi-solution structures and stability regions. A disadvantage is that although the method works accurately in the state space, a mapping of its results into the parameter space is not a straightforward and accurate operation.

Hypercomplex power flow extensions allow reformulating the power problem so that the Jacobian matrix of the reformulated problem becomes non-singular along the power flow feasibility boundary so that the boundary can be explored using conventional numerical methods. A technique developed in Russia[8] uses a combination of the complex and complex conjugate power flow equations along with the assumption that the complex and complex conjugate values of nodal voltages are independent variables. A similar technique developed in Ukraine assumes that the active and reactive components of the nodal voltages are complex numbers.

There is a *progression from one-directional methods* estimating the voltage stability margin in a specified direction *to multi-directional methods* evaluating the distances to instability, and further from the multi-directional methods *to the methods exploring the entire voltage security region* in the parameter space. In the market-driven systems, where the generation dispatches vary, the interactions between the various stresses can be accounted for by sensitivity methods or multi-directional and voltage security region techniques. *The use of power flow existence criterion* bears a potential danger of overestimating the actual voltage security margin in situations where the saddle node bifurcation, Hopf bifurcation, or transient stability conditions are violated before the power flow equations become inconsistent. Due to this consideration, the state-of-the-art methodology should be based on more precise voltage stability criteria.

---

[7] REI – Radial Equivalent Independent
[8] By A. M. Kantorovich

3. Overview of Existing Tools

P-V and V-Q simulation capabilities are provided by almost all industrial-grade VSA tools including ABB-VSA, PSS/TPLAN (Siemens), VSAT (Powertech), VSTAB (EPRI) and other applications as described in this section. An overview of voltage security assessment is provided below.

3.1. Off Real Time Tools

ABB Voltage Security Assessment (ABB-VSA): This application computes the voltage collapse P-V curves and critical operating MW limit for increasing loading condition both for the real time network condition as well as for worse contingencies[9]. In addition to the prediction of this critical point, ABB-VSA determines the set of weakest load flow buses in the system that exhibit the worst voltage drops, thus contributing to voltage collapse.

PSS/E Version 30 (Siemens) includes an additional fully automated feature that allows user to determine real power transfer or load level limit using P-V analysis or determine reactive margin with V-Q analysis. For the automatic contingency analysis, the TPLAN non-divergent power flow is used. For the automatic P-V and V-Q analyses, the IPLAN language[10] script is used. For the post-contingency P-V and V-Q analyses, the Inertia/Governor Load Flow algorithm is used. In this algorithm, the speed governor action is modeled, as well as all automatic actions controlling voltages and frequency in the zero to three minute time frame.

VSAT (Powertech Labs, Inc.): The Powertech voltage security software provides the following capabilities: contingency analysis based on voltage security margin; transfer limits calculation between a source and a sink and between any 3 sources/sinks, voltage level, reactive power, and thermal limits; P-V and V-Q analyses; modal analysis, and remedial actions. Powertech has also developed a near real time application of the DSA Tools described below.

VSTAB, Version 5.2 (EPRI): VSTAB uses power flow based steady-state techniques for stability analysis. VSTAB automates contingency analysis and conducts P-V and V-Q simulations. VSTAB also performs a modal analysis by calculating smallest eigenvalues.

NEPLAN – Voltage Stability (BCP Busarello+Cott+Partner Inc., Switzerland): NEPLAN software implements V-Q analysis, P-V analysis, V-Q sensitivity analysis and modal analysis functionalities. NEPLAN – Voltage Stability helps to identify weak buses, areas, and branches, voltage sensitivity and voltage stability indices. The tool also allows selecting measures to increase voltage stability margin.

WPSTAB (National Technical University of Athens, Greece) is designed for the purpose of a long-term voltage stability and contingency evaluation. WPSTAB uses the Quasi Steady State approach based upon the time-scale decomposition of power system dynamics and a simplified representation of short-term dynamics, when focusing on long term phenomena. This program is used for the in-depth voltage stability analysis in the European Union OMASES project.

3.2. Real Time Tools

ABB's PSGuard: PSGUARD is a phasor measurement based platform that extends the basic functionality of Wide Area Measurement Systems to include real-time voltage stability assessment capability across key transmission corridors solely based on local measurements. It does this by estimating the amount of

---

[9] R. Masiello, "Utilities Must Leverage Existing Resources and Upgrade Technology to Avoid Future Blackouts", Electric Energy T&D Magazine, pp. 44-47. May/June 2004.

[10] The IPLAN language is used to control the host PSS/E program.

additional active power that can be transported on a transmission line or corridor without jeopardizing voltage stability.

Online application of DSA Tools (Powertech Labs, Inc., Canada): It conducts near-real-time security assessment based on the state estimator output. The DSA package runs voltage, transient, and small-signal analyses. The tool identifies violations, transient voltage and frequency dips, critical contingencies, and required remedial actions. Simplified analytical techniques are not used. The Powertech software can be integrated with the Energy Management System (EMS).

EPRI CAR Project: The Community Activity Room (CAR) describes the static security region calculated using a full AC power flow model or a linearized DC power flow model. The CAR uses the MW power injections at each bus as the independent variables and expresses the line flows through these variables. This eliminates the intermediate step of computing bus voltages and angles as would normally be required to solve a load flow. With the direct equations relating line flows to bus injections, it is then possible to express the line flow inequality constraints as functions of bus injections. The Community Activity Room's boundary is defined to be the intersection of all sets of constraints for the normal system topology and for all single branch contingency conditions. The CAR boundaries can be described using either deterministic or probabilistic approaches. The Community Activity Room can be used for online monitoring.

QuickStab (Energy Consulting International, Inc.): QuickStab provides a quick evaluation of the maximum loadability for a user-specified security margin. It also helps to identify generators and inertias that may cause instability. QuickStab has been integrated with EMS/SCADA systems as a real time tool.

ASTRE (University of Liège): The ASTRE software solves the base case, stresses the system in a pre-contingency situation, to simulate energy transactions, and filters out harmless contingencies. Security limits are determined through binary search organized in different ways. Beside security limit calculation, analysis and diagnosis facilities are provided.

3.3. Some Limitations of Existing Tools

▪ Many existing tools use *the power flow existence criterion* to compute the boundary. This has the dangerous potential to overestimate the actual voltage security margin in situations where the saddle node bifurcation, Hopf bifurcation, or transient stability conditions are violated before the power flow equations become divergent.

• The limitations of P-V/Q-V plots that represent the load versus the voltage of a selected bus become apparent when voltage collapses are not concentrated in a few buses. Some voltage collapses are regional or involve the entire system. P-V curves are calculated using the power flow solutions by step-by-step increasing the loads. The "nose point" of the curve corresponds to the maximum power which can be delivered to the load. The bus voltage at this point is the critical voltage. If the voltage of one particular bus approaches the nose point faster compared to the other buses, it is assumed that the system voltage stability margin is limited by this bus. This information does not capture the extent to which all the variables participate in the voltage collapse.

4. Survey Summary and Recommendations

4.1. Survey Overview

CERTS/EPG formulated a survey to reach out to the experts in the field of voltage security for comments, information, suggestions, and recommendations related to the VSA project. The surveys were sent to fifty one experts in universities and in the power industry. Sixteen reviewers responded and their responses are summarized in Table 1. Eight of these respondents are from the power industry and eight are from academia. Four proposals for commercial software were received from Bigwood, V&R, NETSSS, and ECI.

Table 1: Analysis of Survey Trends

ISSUE	RESPONSES / COMMENTS	CONCLUSION
Voltage Security Assessment (VSA) (Hyperplanes for security regions)	- Online hyperplane possible - Not as unproven as interior point methods. - Ideally suited for phenomena that is local.	Hyperplanes well suited for VSA
Methodology for computing hyperplanes	- Loading & Generation Direction needed. - Stress path until voltage collapses. - At collapse, determine local boundary.	Use left eigenvector approach
Direct versus Time-domain methods	- Time domain iterative methods are proven and robust, capable of handling intermediate discrete actions/events. Example: Generator limits being reached Direct methods rely on simplistic models	Direct Method could be used for fine-tuning the security boundaries after an iterative set of continuation power flows
Weak elements identification	- Voltage collapses are concentrated in certain regions in the sense that the voltage falls more in those regions. There is no single element that collapses. That is, voltage collapses occurs system wide with varying participation from all the system buses.	The participation is computed from the right eigenvector of the Jacobian evaluated at voltage collapse corresponding to the zero eigenvalue.

4.2. Summary of Responses

The consensus opinion was that the hyperplane approach to defining security regions was ideally suited for voltage instability assessment. Voltage instability is more of a local area/region phenomenon. Several participants in the survey felt that full blown time domain classifiers should augment the algorithms that utilize Direct Methods. An engineer from a utility in Northern California said that it was not clear how switching conditions could be revealed without "time domain" simulations. A utility from the South shared its experience that it was unable to develop suitable production metrics because of the integration of both continuous (load growth) and non–continuous (contingency) factors into a single metric. The computational methods to be used in VSA could be grouped into 2 broad classes – the Iterative Approach using Continuation Power Flows and the Direct Method. The Direct Method does not provide information on any discontinuous events when the stress parameter is increased. These discontinuous events occur when a thermal, voltage or reactive limit is reached.

4.3. Conclusions

The majority of responses favor the use of the hyperplane approach in determining Voltage Security Assessment.   Also, the majority of respondents do not see hyperplanes suitable for determining Dynamic Voltage Assessment at this time. Small Signal Stability Analysis is considered to be a good first step for Wide Area Stability Monitoring and assessment using phasor measurements.

4.4. Recommendations

The primary recommendation for such a tool is to use the hyperplane approach in computing security regions for Voltage Security Assessment. Others are:

- The computational engine for CA ISO's VSA is recommended to be the Continuation Power Flow. This tool has been tested and proven by several researchers in commercial and non-commercial software.

- An alternate recommendation is a hybrid approach, where a Direct Method could be used for fine-tuning the security boundaries after an iterative set of continuation power flows.

5. CERTS Real-Time Voltage Security Assessment Algorithms

The overall proposed roadmap and framework for the project was based on the literature review and survey results, and formulated through discussions with CA ISO and with active participation of CERTS consultants Dr. Yuri Makarov and Prof. Ian Dobson over conference calls and meetings in Pasadena (August 25-26, 2005) and in Madison (September 9, 2005).

	Phase 1: TO 21	Phase 2: RTGM 2005	Phase 3: RTSO 2006-07
Input Data Requirements		Utilization of CA ISO PTI Cases Utilization of CA ISO GE Planning Model Cases	Research & evaluate utilization of CA ISO CIM data
Algorithms Research	(1) VSA survey & framework based on input from academia and utilities (2) Contingency analysis capabilities (3) Prototype functional specification	Survey recommended algorithms: (1) Continuation Power Flow (2) Hyper planes (3) Bus participation factors in voltage collapse to identify most affected points/regions (4) Compute sensitivities with respect to voltage set points & generator VAR limits	(1) Enhancements to Continuation Power Flow (2) Use of direct methods (3) Implement Boundary orbiting technique
Prototype Development And Test		Validate survey recommended algorithms using Humboldt and San Diego areas	Demonstrate VSA for Southern California (or other) Region
	Contract #500 - 99 -013: BOA 20	Contract #500-02-004: MR-036	**Current Contract #500-02-004 MR-041**

CA ISO Production Quality VSA Functional Specification

CERTS
Consortium for Electric Reliability Technology Solutions

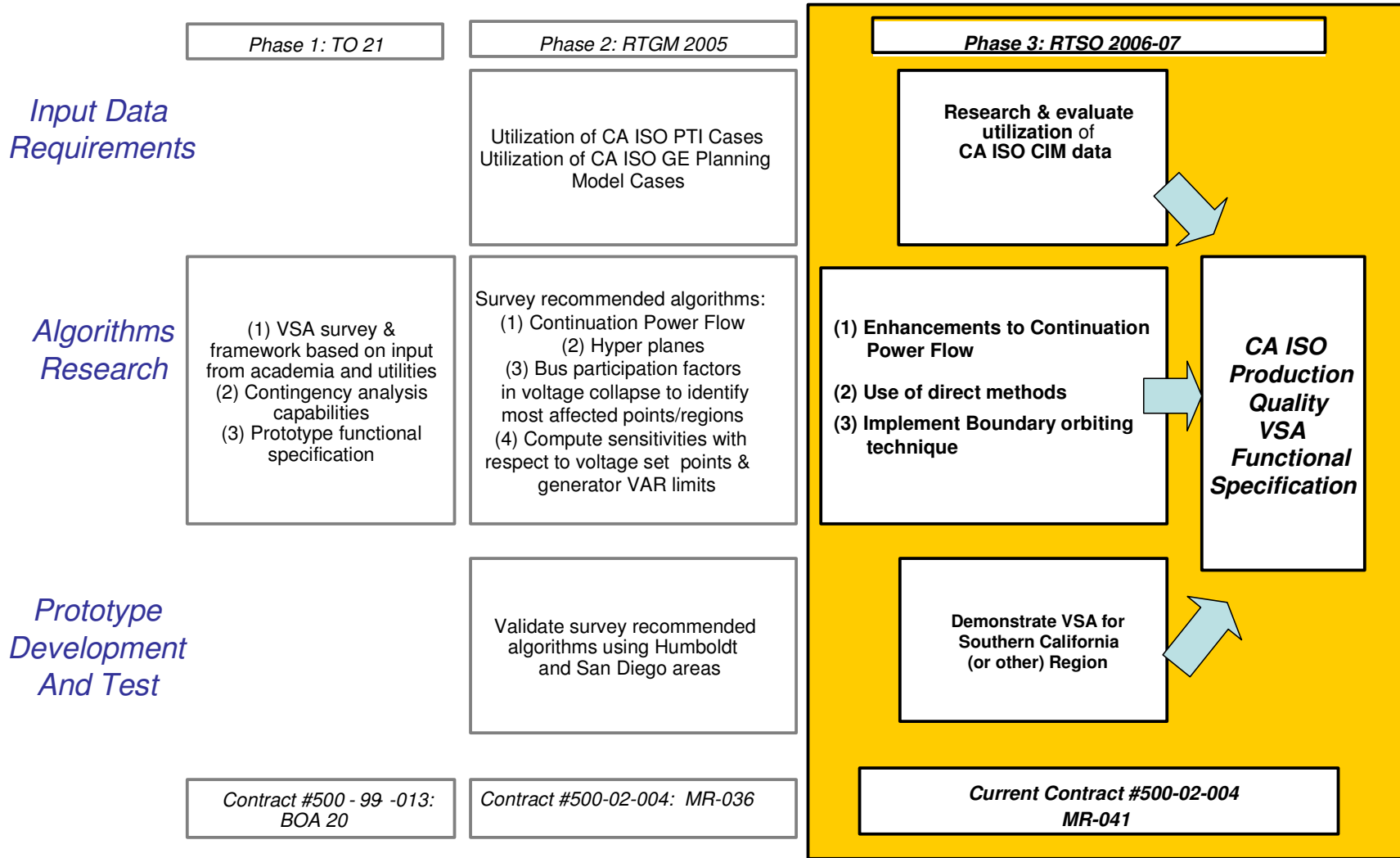✳ **E**lectric **P**ower **G**roup

Figure 1: Multi Year Development Roadmap for CA ISO Voltage Security Assessment (VSA) Project

The roadmap consists of three task tracks focusing on different aspects of the project including data requirements, algorithms research, and prototype development & testing. The multiple phases are a systematic progression starting with initial research, algorithm development and proof-of-concept simulations, and data integration and project expansion. The project time span was two years (2005-2006) with the potential expansion for the future years. The overall framework and the algorithmic building blocks (such as the Continuation Powerflow, Hyperplane Approximations, Direct Methods, etc) and their technical details are described in the sections to follow.

5.1. RTVSA (Real-Time Voltage Security Assessment) Framework

Based on CA ISO's analysis, the most promising method for determining the available voltage stability margin in real time is based on piece-wise linear approximation of the voltage collapse boundary in coordinates of independent power system parameters. The approximating conditions are calculated off-line as a set of inequalities specific for each analyzed contingency:

$$\begin{cases} a_{11}P_1 + ... + a_{1n}P_n + b_{11}Q_1 + ...b_{1n}Q_n \leq c_1 \\ a_{21}P_1 + ... + a_{2n}P_n + b_{21}Q_1 + ...b_{2n}Q_n \leq c_2 \\ ... \\ a_{m1}P_1 + ... + a_{mn}P_n + b_{m1}Q_1 + ...b_{mn}Q_n \leq c_m \end{cases} \quad (1)$$

The number of constraints m and the number of parameters P and Q included in each constraint are expected to be limited. Each face of the region approximates a part of the nonlinear region's boundary. The advantages to the proposed approach are:

- Fast and Convenient assessment: Having constraints (1) pre-calculated offline for each analyzed contingency, it is very easy to quickly determine in real time:
  - o Whether the operating point is inside or outside the security region (by making sure that all approximating inequalities are satisfied)
  - o Which constraints are violated (by identifying violated inequalities), and
  - o What the most limiting constraints are (by calculating the distance from the current operating point to the approximating planes – see below).
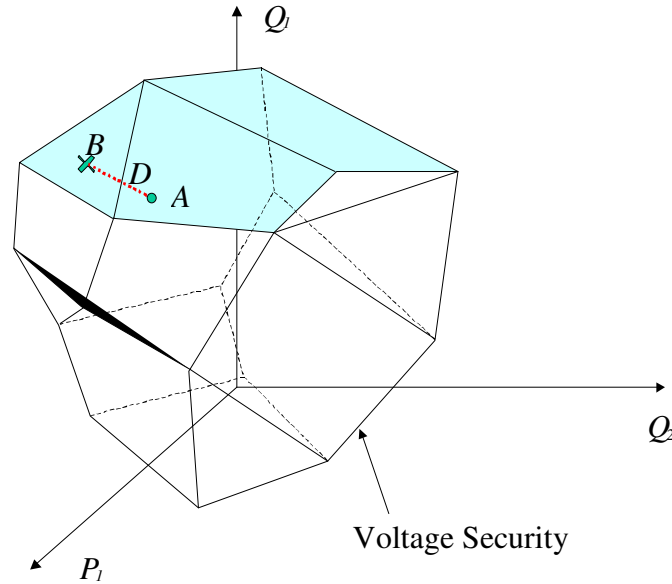
Figure 2: Conceptual view of Voltage Security Region

- Easy-to-Calculate Security Margin: The distance d from the current operating point A to the nearest constraint face B determines the MVA security margin[11]:

$$d_i = \frac{a_{i1}P_1^0 + ... + a_{in}P_n^0 + b_{i1}Q_1^0 + ... + b_{in}Q_n^0 - c_i}{\sqrt{a_{i1}^2 + ... + a_{in}^2 + b_{i1}^2 + ... + b_{in}^2}}$$

Where the current operating point $A = \left[P_1^0, ..., P_n^0, Q_1^0, ..., Q_n^0 \right]$

The percent margin for each constraint i can be obtained based on a pre-established minimum admissible "MVA distance to instability" d^*:

$$d_i^\% = \min \left\{ \begin{array}{l} \dfrac{d_i}{d^*} \times 100\% \\ 100\% \end{array} \right\}$$

The resulting stability margin corresponds to the minimum distance, i.e. the distance to the closest constraint face:

$$D = \min_{(i)} d_i^\%$$

- Online computation of Parameter Sensitivities: The *normalized coefficients* of the set of hyperplane equations denoted by (1) are sensitivities that can be interpreted in several ways. These coefficients can be calculated trivially by the following mathematical expressions:

---

[11] We assume that the region is convex.

$$\frac{\partial D}{\partial P_j^0} = \frac{a_{ij}}{\sqrt{a_{i1}^2 + ... + a_{in}^2 + b_{i1}^2 + ... + b_{in}^2}}$$

$$\frac{\partial D}{\partial Q_j^0} = \frac{b_{ij}}{\sqrt{a_{i1}^2 + ... + a_{in}^2 + b_{i1}^2 + ... + b_{in}^2}}, \; j = 1, ..., n$$

where D is critical vector $\vec{D} = \vec{AB}$ - see Figure 2.

The different representations of these coefficients include:

1) The locations in the network where the most sensitive controls are needed

2) The left eigenvector nullifying the power flow Jacobian matrix at the point of collapse

3) This eigenvector has an identical representation to *Lagrangian multipliers*[12] at PoC

5.2. Algorithms Overview

The important concepts that are used in the algorithm are stress direction (procedure), descriptor variables, state space, and parameter space.

The *stress direction (procedure)* specifies how the system parameters change from their base case values as a function of a scalar amount of stress. For example, generation and load participation factors can define a stress direction and the amount of generation can give a scalar amount of stress and these together can specify the changes in the bus power injections that is, any system state along the stress direction can be associated with certain value of a stress parameter such as the percent of the total load increase in an area. Each specific direction and value of the stress parameter uniquely defines the system state. This implies certain fixed patterns for varying the system generation and loads (for example, load participation factors, sequence of generator dispatch, and others – detailed examples can be found in this report). Stress directions can include some local system stresses addressing a particular voltage stability problem area, and global stresses such as the total load growth and the corresponding generation redispatch in the system.

Descriptor variables reflect the most influential or understandable combinations of parameters (or derivative parameters) that influence the voltage stability margin. Examples are the total area load, power flows in certain system paths, total generation, and others (the system operating nomograms' coordinates are good examples of descriptor parameters). In the simplest case, descriptor parameters can include some primary system parameters such as nodal voltages and nodal power injections. Descriptor variables help to adequately address global and local voltage stability margins without involving thousands of primary parameters. Certain subsets of descriptor variables can correspond to some local voltage stability problem areas.

The *state space* includes all system nodal voltage magnitudes and voltage phase angles.

The (independent) *parameter space* includes all nodal power injections (for P-Q buses) and real power injections and voltage magnitudes (for P-V buses).

The voltage stability boundary can be comprehensively (and uniquely) described in the parameter space (and the state space), but in this case the description would involve thousands of variables. Descriptor

---

[12] This representation is well suited to imply a 'Locational price' for an ancillary service such as the distance to voltage collapse specified in terms of dollars. *Lagrangian multipliers* specify the sensitivity of the constraints so that a constrained optimization problem becomes an unconstrained optimization problem – see Eric W. Weisstein. "Lagrange Multiplier" from MathWorld - A Wolfram Web Resource. http://mathworld.wolfram.com/LagrangeMultiplier.html

parameters help to reduce the dimensionality of the problem by considering the most influential combinations of parameters (or derivative parameters).

The *descriptor parameter space* includes all descriptor parameters. Since the points in the descriptor parameter space can be mapped into the points of the parameter and state spaces in many different ways (because of the limited number of descriptor parameters space dimensions), certain fixed system stress procedures should be introduced to make this mapping adequate and unique.

The developed RTVSA algorithm operates in the parameter space or descriptor space as described in Section 5.9.

The developed RTVSA algorithms consist of the following steps (which has been illustrated in a flowchart under Figure 3):

1. **Initial system stressing procedure** for a given stress direction **to reach a vicinity of the Point of Collapse (PoC)** in this direction. This step is implemented using the Parameter Continuation Method described in Section 5.3. The Continuation Method is one of the most reliable power flow computation methods; it allows approaching the PoC and obtaining the initial estimates of system state variables needed for the subsequent steps. The selected form of the continuation methods includes predictor and corrector steps.

2. **The direct method** – see Section 5.4 – is used then **to refine the PoC location** along the initial stress direction (the continuation method would require multiple iterations to find the PoC with the required accuracy). At least one of the power flow Jacobian matrix eigenvalues must be very close to zero at the PoC.

3. **The inverse iteration method or Arnoldi algorithm** is applied **to find the left eigenvector corresponding to the zero eigenvalue at PoC** – see Section 5.5. The left eigenvectors are used to build the set of approximating hyperplanes.

4. **The stability orbiting procedure is then applied to trace the voltage stability boundary along a selected slice.** This procedure is a combination of a predictor-corrector method and the transposed direct method. Details are given in Section 5.6.

5. In case of divergence, the algorithm is repeated starting from Step 1 for a new stress direction predicted at the last iteration of the orbiting procedure. Divergence may be caused, for example, by singularities of the stability boundary shape along the slice.

6. For a given voltage stability problem area and the corresponding descriptor parameters, **the "sliced bread procedure" is applied to explore the voltage stability boundary and build the set of approximating hyperplanes** – see Section 5.7.

7. The approach to build the minimum set of hyperplanes based on the desired accuracy of the approximation is given in Section 5.8.

8. The algorithm described above is implemented in the descriptor space as described in Section 5.9.

Input
- Converged Load Flow Solution
- Single Stressing Direction and associated RASs
- Descriptor Variables
- Contingencies

Parameter Continuation Method (Predictor - Corrector) Including Voltage/Var Limit Check

Reach Vicinity of Point of Collapse

Direct Method

PV Curve Showing a Load Voltage
(Indicates Point of Collapse Solution)

New Stressing Direction (gamma, eta)

- Security Region Parameters (E_i & E_j)

Input

Output Data

- Point of Collapse Solution
- Left Eigenvector
- Right Eigenvector
- Load Margin
- Weak Elements
- Corrective Actions
- Sensitivities

Boundary Orbiting Method With Voltage/Var Limit Check

Convergence of Solution?

YES

Tracing of Boundary Complete?

NO

NO

YES

2-D Security Region in Injection Space

2-D Security Region for two Load Buses
(Shown in Parameter Space)

Mapping of Nomogram (Injection 4 Descriptor Space)

- Descriptor Parameters

Input

Output Data

- 2-D Nomogram

Slice Bread Procedure

3-D Security Region
(Slice Bread Procedure)

Note: The above procedure involves contingency analysis and screening and a security region is formed for the most binding contingency
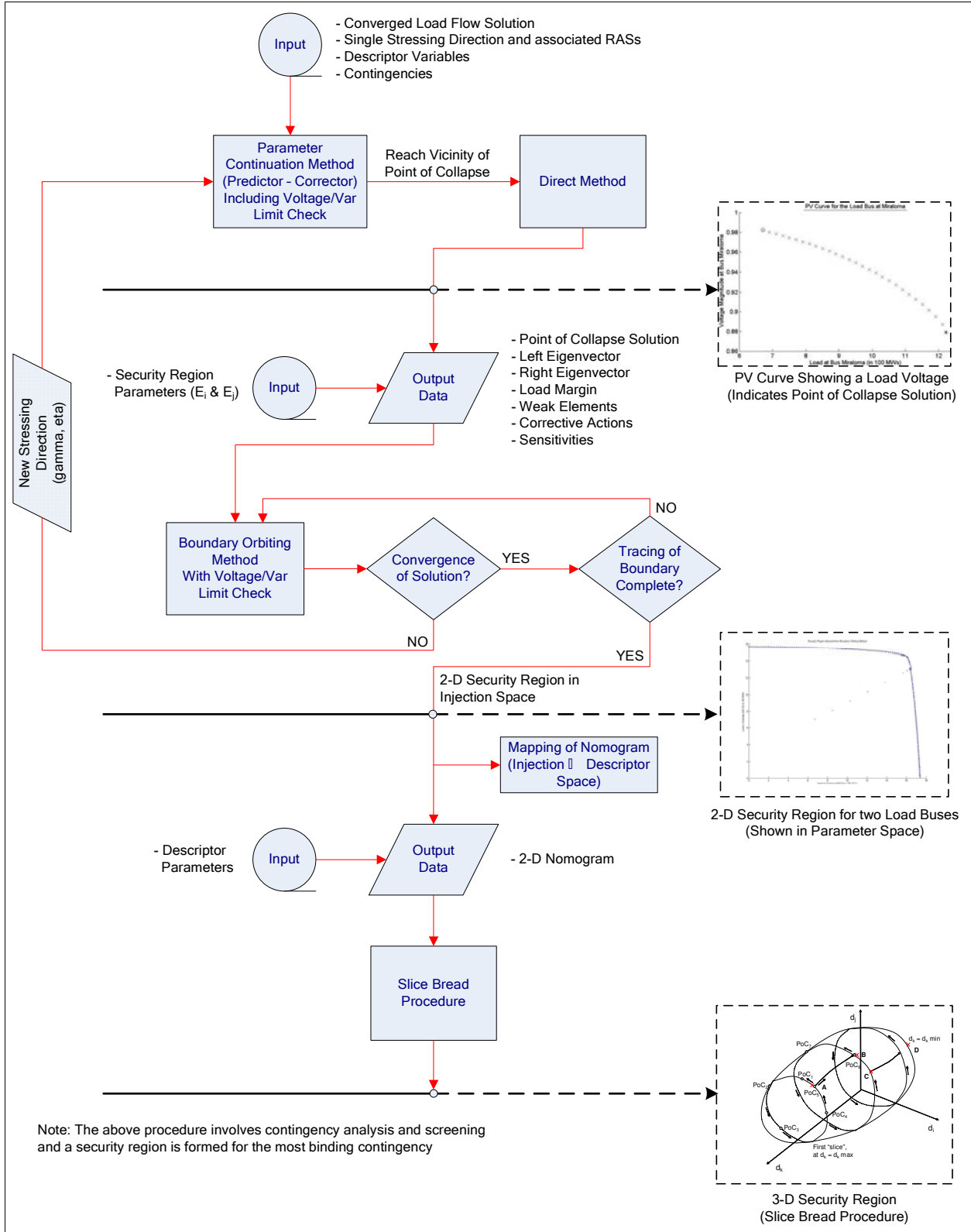
Figure 3: RTVSA Algorithms Flowchart

The developed RTVSA algorithm performs voltage security assessment calculations under both offline and real-time modes.

The *offline calculations* produce an approximated voltage stability region (a 2-D, 3-D, or a higher dimensional nomogram) bases on multi-directional stressing situation presenting the interaction and tradeoffs between different stressing directions. The pre-calculated voltage stability region is an inner intersection of stability regions for the set of user-specified contingencies. The offline calculations should be conducted periodically (ideally, several times a day) to update the approximated voltage security region and to reflect the most recent changes in the system.

The *real-time calculations* are conducted in real time (after each converged State Estimation cycle) to determine the current or future position of the system operating point against the walls of the approximated voltage stability region, and to calculate such essential security information as the available stability margin (distance to instability), the most limiting contingency, the most dangerous system stress directions, weak elements causing potential instability, and the recommended preventive and enhancement controls that help to increase the margin in an efficient way.

Note: The *offline* calculations can also be conducted in real time if a few stressing directions representative of the actual system loading, given by the real time dispatch schedule, planned outages, and load forecast, and/or predetermined stresses are to be considered separately. In such a scenario, the available security margins, distance to instability, the most limiting contingency, weak elements causing potential instability, and the recommended preventive and enhancement controls that help to increase the margin in an efficient way can be obtained in real-time using the algorithms proposed in this document.

5.3. Continuation Method

The CERTS-RTVSA (Real Time Voltage Security Assessment) algorithm is based on methods that were originally used in the NSF-PSERC algorithm found at http://www.pserc.cornell.edu/tcc/. The algorithm is a variation of the predictor-corrector type of the continuation power flow.

In the generic continuation power flow framework, $\Phi(z)$ is **n+1** dimensional and represents the power flow equations augmented by a parameter $\Delta\lambda$ that is free to change, Δx is the **n** dimensional change in the state vector, $\Delta\lambda$ is **1** dimensional and Δz is **n+1** dimensional.

$$\Delta z = [\Delta x, \Delta \lambda]^{\top}$$

$$\frac{\partial \Phi}{\partial x} \Delta x + \frac{\partial \Phi}{\partial \lambda} \Delta \lambda = 0$$

where $\dfrac{\partial \Phi}{\partial \lambda}$ represents the stress vector

In the nomenclature used here, the 'Parameters' are defined as injections such as real power P_i and reactive power Q_i inputs, and the `States' are defined as voltage magnitudes V and angles δ (Note: The 'Descriptive' variables that classify the security regions could either be a linear combination of Parameters or States, or Cut Set Power Flows).

The system Φ above is under-determined and the Tangent Vector Δz is non-unique, unless one further constrains one of its elements. In the Ajjarapu-Christy [55] algorithm, the variable that moves the fastest in the previous iteration is constrained. If $\Delta\lambda$ is always constrained, then the reduced Tangent Vector can be defined as

$$\frac{\Delta x}{\Delta \lambda} = -\frac{\partial \Phi}{\partial x}^{-1}\frac{\partial \Phi}{\partial \lambda}$$

Note that $\partial \Phi / \partial \lambda$ is the vector of "participation factors" of the set of buses forming the Sink. In other words, if the change in Net System Load represented by $\Delta \lambda$ moves by 1 MW, then $\partial \Phi / \partial \lambda$ denotes the distribution of the 1 MW across the buses constituting the Sink.

Additionally, the sinks and source have distinctly different roles in the computations used to apply stress. The sinks are considered parameters of the model while the sources are variables. Stress is applied by incrementing the stress sinks and then solving the power flow problem to determine the variables.

The proposed CERTS-RTVSA algorithm uses a variation of the above method which is described below.

5.3.1.   Predictor & Corrector Equations and Algorithms

Predictor Equation:

$$\begin{cases}\dfrac{\partial \Phi}{\partial z}\Delta z = 0 \\ e_i^t \Delta z = 1\end{cases} \Leftrightarrow \begin{bmatrix} \dfrac{\partial \Phi}{\partial z} \\ ----- \\ e_i^t \end{bmatrix}\Delta z = \begin{bmatrix} 0 \\ --- \\ 1 \end{bmatrix}$$

where e_i^t is a zero string with only **i**[th] element equal to 1.

Corrector Equation:

Use Newton Raphson to solve $\Phi(z) = 0$
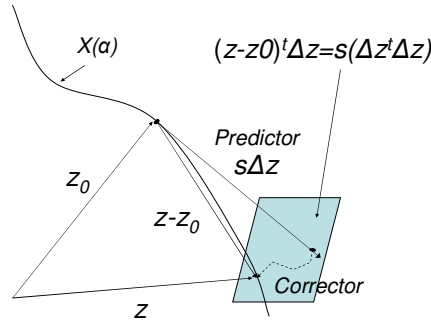
$$\Delta z_i = 0$$

Figure 4: Predictor and Corrector Steps

The main steps in the CERTS-RTVSA predictor algorithm are:

1. Solve the predictor equation and normalize the length of the composite predictor vector Δz by division by $\sqrt{\Delta z^t \Delta z}$

2. Select the step size length **s** based on the maximum values $\Delta\delta_{max}$ and ΔV_{max} and the current value of the step multiplier γ.

   Select **s** so that $s \max\{\Delta V\} = \gamma\Delta V_{max}$, while $s \max\{\Delta\delta\} \leq \gamma\Delta\delta_{max}$,

   $\qquad$ or $s \max\{\Delta\delta\} = \gamma\Delta\delta_{max}$, while $s \max\{\Delta V\} \leq \gamma\Delta V_{max}$,

   whatever is achieved first. Note that in both the **predictor[†]** and the **corrector[‡]** equation the **i**[th] index corresponds to the state that first reaches the maximum.

3. Scale the predictor vector Δz by *s* so that $\Delta z^* = s\Delta z$

4. Use Δz^* for solving the corrector equation

5. If the power flow for the corrector equation **does not** converge

   a. **Halve** the step multiplier γ

   b. Do **not** update z

   c. Go to Step 2

6. If power flow for the corrector equation **does** converge

   a. **Halve** the step multiplier if (γ is **greater than** γ_{min} & Δλ changes sign). Go to Step 2

   b. Update z and Go to Step 1

7. Criteria for stopping

   a. Stop if γ is **less than** γ_{min} in Step 5

   b. Stop if Δλ changes sign & γ is **less than** γ_{min} in Step 6

The maximum value of the step size is a criterion for limiting the deviation in states between each iteration. It is specified separately in per unit (pu) voltage and electrical degrees, $\Delta\delta_{max}$ and ΔV_{max} and has been selected as 0.08 radians (5 deg) and 0.05 pu based on engineering experience and experiments. Additionally, the initial step multiplier γ will be halved in the algorithm depending on

1. Whether the power flow is non-convergent
2. Whether γ is greater than the specified minimum multiplier γ_{min}

5.3.2. Criteria to Determine Proximity to PoC

1. Small Elements on the Diagonal of the Triangularized Power Flow Jacobian Matrix
2. Power Flow Jacobian Matrix Condition Number
3. Minimum Singular Value

Some of the disadvantages of the above criteria are that these do not capture the sudden changes of power flow equations due to discrete events such as capacitor switching of handling reactive power constraints on generators. It misses the PoC points where the power flow become inconsistent without a singularity of the power flow Jacobian matrix due to discrete events mentioned above. In addition (2) & (3) are also computationally expensive. Some of the problems outlined here that relate to difficulties in determining the exact PoC are alleviated by the Direct Method, described next.

5.4. Direct Methods to Calculate the Exact Bifurcation Point

The exact location of the PoC can be calculated by solving the following system:

$$\begin{cases} F(x) + \beta D = 0 \\ J(x)R = 0 \\ R^t R = 1 \end{cases}$$

where $J(x)$ is the power flow Jacobian matrix and R is the right eigenvector corresponding to the zero eigenvalue of $J(x)$. The loading direction D is exactly the same as the one used in the predictor-corrector procedure.

To solve the above set of equations, it is important to select good initial guesses for unknown parameters x, β, and R. For x and β, use the values produced by the predictor-corrector method nearby the PoC. For R, a good initial guess would be the normalized increment of state variables Δx nearby the bifurcation point. An example is the difference between two successive iterations close to PoC, as given below.

$$R_0 \approx \frac{x_i - x_{i-1}}{\|x_i - x_{i-1}\|}, \quad x_i \to \text{PoC}$$

This recommendation is based on the fact that the trajectory of the state variables tends to the right eigenvector R in a small neighborhood of the PoC.

5.5. Hyperplanes at the Point of Collapse

To determine the approximating hyperplane, the left eigenvector L is needed. This vector is an orthogonal vector with respect to the power flow feasibility boundary at the PoC in Figure 5. In order to calculate the left eigenvector, an inverse iteration technique is recommended[13].
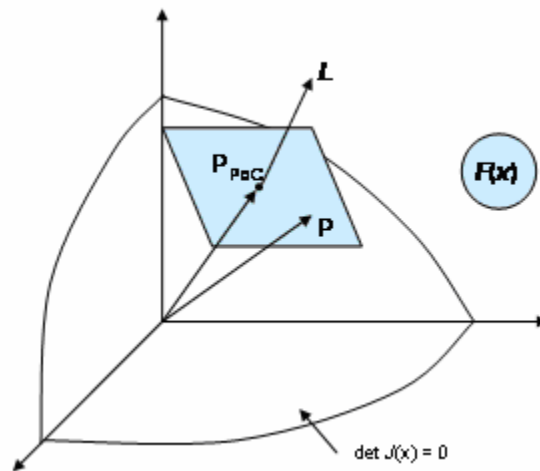

Figure 5: Left eigenvector of *J*(*x*)

---

[13] The RTVSA code was implemented using Arnoldi algorithm

The algorithm behind the inverse iteration method is as follows. Consider the linear system:

$$\left[J^{t}(x \to x_{PoC}) - \lambda_{i-1} \cdot E \right] \cdot \tilde{L}_{i} = L_{i-1}$$

where $J(x \to x_{PoC})$ is the power flow Jacobian matrix calculated near the PoC; λ_{i-1} is an estimate of an eigenvalue; E is the identity matrix, and L_{i-1} and $\tilde{L}_{i}$ are successive estimates of the left eigenvalue. It is recommended to normalize vector $\tilde{L}_{i}$ at each iteration as follows:

$$L_{i} = \frac{\tilde{L}_{i}}{\left\| \tilde{L}_{i} \right\|}$$

The eigenvalue estimate λ_{i} can be improved by applying the following correction:

$$\lambda_{i} = \lambda_{i-1} + \frac{1}{\tilde{L}_{i} \cdot L_{i-1}}$$

In the vicinity of the PoC, the initial guess of λ should be selected as zero, $\lambda_{0} = 0$.

The inverse iteration method usually demonstrates quick convergence. The exception is the case with closely located eigenvalues. Bad selection of the left eigenvector may slow down the iteration process. The recommended initial choice is $L_{0} = D$ (loading direction).

The underlined tangent hyperplane *p* = *F*(*x*) can be easily found by applying the following formula:

$$L^{t} \cdot [p - PoC] = 0 \to p = F(x)$$

Note that:

- The approximating hyperplane is a tangent plane with respect to the load flow feasibility boundary if it is smooth at the PoC.

- If the load flow feasibility boundary if it is convex, the entire tangent hyperplane lies outside the boundary. This prevents the direct use of the tangent hyperplane as the approximating hyperplane because of the overestimation of the actual margin – see Figure 6. Instead, a more conservative approximation by secant hyperplanes is suggested.

- *L* is a perpendicular vector with respect to the hyperplane.

- The hyperplane is actually a (*n* – 1) subspace of the *n*-dimensional space *F*(*x*).

The following section describes the procedure to obtain an approximation of the power flow feasibility region by secant approximating hyperplane. It is assumed that the procedure is performed in the space of *k* parameters (nodal injections or descriptive parameters in the sequel) *p* = *{p₁, p₂... pₖ}*, and that the process is organized for a pair of parameters *pᵢ* and *pⱼ* that are varied while the rest are kept constant.
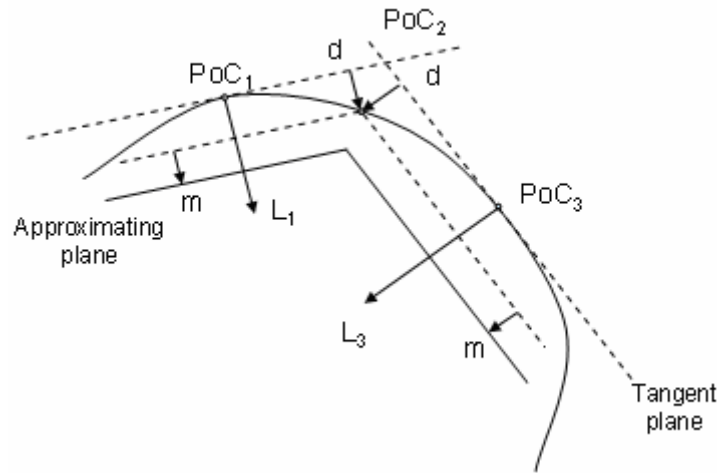
Figure 6: Tangent and approximating hyperplanes

Effectively, this means that the power flow feasibility boundary is cut by a plane, and that we consider one cut set ("slice") at a time to build the entire approximation. The following in the hyperplane building procedure:

1. Suppose we determined the first point of collapse PoC_1, the normalized left eigenvector L_1, $\|L_1\| = 1$, and the corresponding tangent hyperplane $L_1^t \cdot (p - PoC_1) = 0$ - see Figure 6.

2. The approximating hyperplane is obtained by parallel shifting the tangent hyperplane along vector L_1 by the distance $(d + m)$, there d and m is the user specified distances. Distance d regulates the accuracy of approximation and the number of required hyperplanes, distance m introduces an additional security margin. The approximating hyperplane equation becomes

$$L_1^t \cdot (p - PoC_1) = d + m$$

3. Now we start moving along the intersection boundary and the cut set plane (p_i, p_j). As it will be described below, this motion can be implemented as another type of the parameter continuation procedure, where the intermediate points of collapse are available.

4. For each intermediate PoC, we will check the distance r to the tangent hyperplane determined at PoC_1. We are looking for a point PoC_2 where this distance is slightly les or equal to the user specified distance d:

$$\mathrm{r} = \frac{\left\| L_1^t \cdot (PoC_2 - PoC_1) \right\|}{\left\| L_1^t \right\|} \le d, \quad r \approx d$$

5. Continue moving in the same direction checking the distance r from the tangent hyperplane to the PoC_2. We ate looking for the PoC_3 where

$$\mathrm{r} = \frac{\left\| L_3^t \cdot (PoC_3 - PoC_2) \right\|}{\left\| L_3^t \right\|} \le d, \quad r \approx d$$

6. Calculate the new approximating hyperplane

$$L_3^t \cdot (p - PoC_3) = d + m$$

7. Repeat the procedure by continuing the motion along the slice and measuring the distance of the hyperplane from the PoC_3, and so on.

5.6. Stability Boundary Orbiting Procedure

This section of the document describes a procedure to orbit the static voltage stability boundary. The procedure includes the following steps (illustrated in Figure 7 below):

- Finding the left eigenvector *L* – this step is repeated one time for the first point found on the boundary that has been already found with the help of the parameter continuation method and the direct method.
- Changing the stress direction to orbit the boundary.
- Predictor step of the orbiting direct method.
- Corrector step of the orbiting direct method.

The last three steps are repeated in the same sequence to follow the boundary.
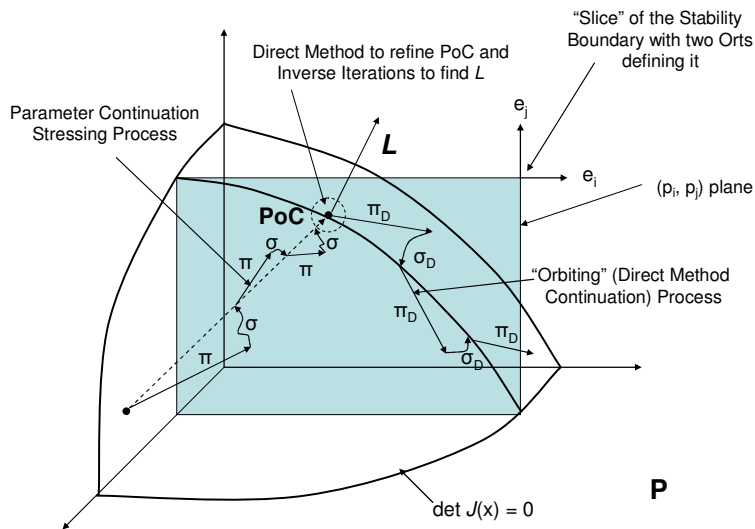
Figure 7: Transition from Parameter Continuation to Orbiting

(π, σ – Predictor and Corrector Steps of the Continuation Method,

π_D, σ_D – Predictor and Corrector Steps of the Orbiting Direct Method)

They are essential parts of the "sliced bread" procedure that has been described in Section 5.7, and have been used along with the hyperplane building and approximation procedure. This procedure does not account for sequential generator loading procedure (i.e. when the generators are loaded one by one following a certain sequence); however, it can be incorporated in the parameter space concept described in section 5.9 of this document.

5.6.1. Finding the Left Eigenvector

In order to calculate the left eigenvector, it is recommended to use the inverse iteration technique as described in section 5.5. The transposed direct method is suggested as an alternative approach.

Transposed Direct Method

The Transposed Direct Method can be applied as an alternative of the inverse iteration method. It consists of solving the system (1) using the Newton-Raphson method.

Transposed Direct Method Equations [2*nbus+1+nPV +2*nbus+1+nPV+1]:

$$F_{D-trans}(x_D) =$$

$$\begin{cases} P(\theta,V) - P_D\beta_1 + T_D'\beta_2 = 0 & \text{- Active Power Balance [nbus]} \\ Q(\theta,V) + Q_{PV} + T_D''\beta_2 = 0 & \text{- Reactive Power Balance [nbus]} \\ \Delta\theta_{RB} = 0 & \text{- Reference Bus Equation [1]} \\ \Delta V_{PV} = 0 & \text{- PV Bus Equations [nPV]} \\ J^t(x)L = 0 & \text{- Singularity Condition [2*nbus+1+nPV]} \\ L^t L = 1 & \text{- Nonzero condition For the Left Eigenvector [1]} \end{cases} \quad (1)$$

Transposed Direct Method Variables x_D [2*nbus+1+nPV +2*nbus+1+nPV+1]:

$$\begin{array}{ll} \theta & \text{- Voltage Phase Angles [nbus]} \\ V & \text{- Voltage Magnitudes [nbus]} \\ \beta_1 & \text{- Source Factors (Distributed Slack Bus Factors) [1]} \\ Q_{PV} & \text{- PV Bus Reactive Power Injections [nPV]} \\ \beta_2 & \text{- Sink Factor (Stress Factor) [1]} \\ L & \text{- Left Eigenvector [2*nbus+1+nPV]} \end{array} \quad (2)$$

Equation set (1) is very similar to the Direct Method equations set except that the last two equations in (1) are written for the left eigenvector L instead of the right eigenvector R.

The recommended initial choice of L is again $L_0 = \begin{bmatrix} T_D' \\ T_D'' \\ 0 \\ 0 \end{bmatrix}$ (stress direction).

5.6.2. Changing the stress direction

We will use equation

$$\Phi(z) = \begin{cases} F(x) + \gamma \cdot e_i + \eta \cdot e_j = 0 \\ J^t(x) \cdot L = 0 \\ L^t \cdot L = 1 \end{cases} \quad (3)$$

Where

$$F(x) =$$
$$\begin{cases} P(\theta,V) - P_D\beta_1 + T_D'\beta_2 = 0 & \text{- Active Power Balance [nbus]} \\ Q(\theta,V) + Q_{PV} + T_D''\beta_2 = 0 & \text{- Reactive Power Balance [nbus]} \\ \Delta\theta_{RB} = 0 & \text{- Reference Bus Equation [1]} \\ \Delta V_{PV} = 0 & \text{- PV Bus Equations [nPV]} \end{cases} \qquad (4)$$

e_i and e_j are unit vectors spanning the "slice" plane (p_i, p_j) - see Figure 7, and $z = [x, L, \gamma, \eta]$.

In (4), parameter β₂ is fixed, and two additional unknown parameters γ and η are added. By varying γ and η, one can explore the entire plane (p_i, p_j).

5.6.3.   Predictor step of the orbiting direct method

Set (3) has one unknown more than the number of equations. It can be used to organize the prediction-correction process.

The predictor equation becomes:

$$\begin{bmatrix} J(x) & 0 & e_i & e_j \\ \frac{\partial}{\partial x}[J^t(x)L] & J^t(x) & 0 & 0 \\ 0 & L^t & 0 & 0 \\ \overline{} & \overline{} & \overline{} & \overline{} \\ & E_r^t & & \end{bmatrix} \cdot \begin{bmatrix} \Delta x \\ \Delta L \\ \Delta\gamma \\ \Delta\eta \end{bmatrix} = - \begin{bmatrix} F(x) + \gamma \cdot e_i + \eta \cdot e_j \\ J^t(x)L \\ L^t L - 1 \\ Step \end{bmatrix} \qquad (5)$$

where E_r is the extended unit vector, and *Step* is the step size. Note that E_r contains 2*nbus+1+nPV +2*nbus+1+nPV+2 elements.

T_D', T_D'' – fixed and equal to the initial loading direction;

β₂ – fixed and equal to the value achieved by applying the direct method procedure;

x – variable, initially set equal to the values achieved by applying the direct method procedure;

L – variable, initially set equal to the vector obtained by the inverse iterations procedure or by the transposed direct method; and

γ, η – variables.

Equation (5) needs to be carried out only once for each predictor step.

5.6.4. Step Selection Procedure

To force the procedure around the boundary, one of the last two elements in E_r (corresponding to either e_i or e_j) must be fixed, and the remaining elements must be zeros.

Algorithm:

1. Find a unit vector that belongs to the "slice" (e_i, e_j) and is orthogonal to L. This can be done by solving the following system

$$L^t \cdot \left(\overline{\gamma} \cdot e_i + \overline{\eta} \cdot e_j \right) = 0$$
$$\left(\overline{\gamma} \right)^2 + \left(\overline{\eta} \right)^2 = 1 \tag{6a}$$

To solve (6a), let us express $\overline{\eta}$ from the first equation in (6a), $\overline{\eta} = -\overline{\gamma} \cdot \dfrac{L^t \cdot e_i}{L^t \cdot e_j}$, and substitute it

into the second equation, $\left(\overline{\gamma} \right)^2 + \left(\overline{\gamma} \right)^2 \left(\dfrac{L^t \cdot e_i}{L^t \cdot e_j} \right)^2 = 1$. Therefore, (6a) has the following solution:

$$\overline{\gamma} = \sigma \cdot \sqrt{\dfrac{1}{1 + \left(\dfrac{L^t \cdot e_i}{L^t \cdot e_j} \right)^2}}$$
$$\overline{\eta} = -\overline{\gamma} \cdot \dfrac{L^t \cdot e_i}{L^t \cdot e_j} \tag{6b}$$

where $\sigma = \pm 1$. Unit vector $\mu = \overline{\gamma} \cdot e_i + \overline{\eta} \cdot e_j$ gives a locally optimal orbiting direction of the steady state stability boundary within the "slice" (e_i, e_j).

2. At the initial orbiting point PoC_0 (Figure 7), assume $\sigma = +1$ and go to the next step. At the subsequent steps, do the following.
   - Assume $\sigma = +1$.
   - Find vector $\mu = \overline{\gamma} \cdot e_i + \overline{\eta} \cdot e_j$ for $\overline{\gamma}$ and $\overline{\eta}$ determined using (6b).
   - Find vector $\xi = \Delta\gamma \cdot e_i + \Delta\eta \cdot e_j$ using $\Delta\gamma$ and $\Delta\eta$ determined at a previous predictor-corrector step.
   - Check the cosine of the angle θ between vectors ξ and μ, $\cos\theta = \dfrac{\mu^t \cdot \xi}{\|\mu\| \cdot \|\xi\|}$.
   - If $\cos\theta$ is negative, reverse signs of $\overline{\gamma}$ and $\overline{\eta}$ (i.e. assume that $\sigma = -1$).

3. Set the last two elements in E_r equal to $\overline{\gamma}$ and $\overline{\eta}$. Set initial guesses $\Delta\gamma = Step \cdot \overline{\gamma}$ and $\Delta\eta = Step \cdot \overline{\eta}$.

The idea behind this step is as follows. The last equation in (5) is $E_r(i) \cdot \Delta\gamma + E_r(j) \cdot \Delta\eta = Step$, where $E_r(i)$ and $E_r(j)$ are the last two elements in E_r. Since they are equal to $\overline{\gamma}$ and $\overline{\eta}$, we have $\overline{\gamma} \cdot \Delta\gamma + \overline{\eta} \cdot \Delta\eta = Step$. This condition will keep $\Delta\gamma$ and $\Delta\eta$ close to the locally optimal orbiting direction $\mu = \overline{\gamma} \cdot e_i + \overline{\eta} \cdot e_j$ as possible, and help to keep the step size closer to the one selected by the User (*Step*). Parameter *Step* must be always positive.

5.6.5. Corrector step of the orbiting direct method

The correction equation looks exactly as (5) with *Step* substituted by zero:

$$
\begin{bmatrix}
J(x) & 0 & e_i & e_j \\
\dfrac{\partial}{\partial x}[J^t(x)L] & J^t(x) & 0 & 0 \\
0 & L^t & 0 & 0 \\
\hdashline
& E_r^t & &
\end{bmatrix}
\cdot
\begin{bmatrix}
\Delta x \\
\Delta L \\
\Delta\gamma \\
\Delta\eta
\end{bmatrix}
= -
\begin{bmatrix}
F(x) + \gamma \cdot e_i + \eta \cdot e_j \\
J^t(x)L \\
L^t L - 1 \\
0
\end{bmatrix}
\tag{7}
$$

Equation (7) needs to be repeated until a convergence solution is obtained for each corrector step.

Vector E_r should be the same as determined in the predictor step.

Note that after each predictor-corrector step, we get a point of the power flow feasibility boundary and the left eigenvector - that is all what is needed for the hyperplane approximation (section 5.5) and the "slice bread" procedure described in the next section.

The corrector step of the orbiting direct method may not converge for various reasons, for example, singularities of the stability boundary shape along the slice. In this case, the VSA algorithms are repeated starting from the Continuation Method (section 5.3) for a new stress direction predicted at the last iteration of the orbiting procedure.

5.6.6. Calculating $\dfrac{\partial}{\partial x}\left[J^t(x)L\right]$

Calculating the matrix $\dfrac{\partial}{\partial x}\left[J^t(x)L\right]$ can be done using the Hessian matrices (described in Appendix A) - second derivatives of the mismatch function $F(x)$. This is what is recommended for the vendor's implementation. To minimize the programming effort to build the prototype tool, approximate expressions can be applied as described below. However, they are more complicated and require more computational effort.

Function $F(x)$ can be represented as its Taylor series:

$$F(x+\vartheta R) = F(x) + \vartheta J(x)R + \frac{1}{2}W_2(\vartheta R, \vartheta R) + \frac{1}{6}W_3(\vartheta R, \vartheta R, \vartheta R) + ...$$

$$F(x-\vartheta R) = F(x) - \vartheta J(x)R + \frac{1}{2}W_2(\vartheta R, \vartheta R) - \frac{1}{6}W_3(\vartheta R, \vartheta R, \vartheta R) + ...$$

(8)

Where $W_2(\vartheta R, \vartheta R)$ and $W_3(\vartheta R, \vartheta R, \vartheta R)$ are the second- and third-order terms of the expansion. It is obvious that $W_2(\vartheta R, \vartheta R) = W_2(-\vartheta R, -\vartheta R)$, $W_2(\vartheta R, \vartheta R) = \vartheta^2 W_2(R, R)$, $W_3(\vartheta R, \vartheta R, \vartheta R) = -W_3(-\vartheta R, -\vartheta R, -\vartheta R)$, and that $W_3(\vartheta R, \vartheta R, \vartheta R) = \vartheta^3 W_3(R, R, R)$.

By subtracting equations in (8),

$$F(x+\vartheta R) - F(x-\vartheta R) = 2\vartheta J(x)R + \frac{\vartheta^3}{3}W_3(R, R, R) + ...$$

(9)

and

$$J(x)R = \frac{1}{2\vartheta}\left[F(x+\vartheta R) - F(x-\vartheta R)\right] - \frac{\vartheta^2}{6}W_3(R, R, R) + ...$$

(10)

Finally, by differentiating (10), one can get

$$\frac{\partial}{\partial x}[J(x)R] = \frac{1}{2\vartheta}[J(x+\vartheta R) - J(x-\vartheta R)] + o^2(\vartheta)$$

(11)

By substituting R by e_k, where e_k is a unit vector,

$$\frac{\partial}{\partial x}[J(x) \cdot e_k] = \frac{1}{2\vartheta}[J(x+\vartheta e_k) - J(x-\vartheta e_k)], \ \vartheta e_k \to 0$$

(12)

Now,

$$\frac{1}{2\vartheta}L^t[J(x+\vartheta e_k) - J(x-\vartheta e_k)], \ \vartheta e_k \to 0 \overset{(15)}{=} L^t\frac{\partial}{\partial x}\{J(x) \cdot e_k\}$$

$$= \frac{\partial}{\partial x}\{L^t \cdot J(x) \cdot e_k\} = \frac{\partial}{\partial x}\{[L^t \cdot J(x)] \cdot e_k\}$$

$$= \frac{\partial}{\partial x}\{e_k^t \cdot [L^t \cdot J(x)]\} = \frac{\partial}{\partial x}\{e_k^t \cdot [J^t(x) \cdot L]\}$$

$$= e_k^t\frac{\partial}{\partial x}[J^t(x) \cdot L]$$

(13)

Row vector $e_k^t\frac{\partial}{\partial x}[J^t(x) \cdot L]$ is the k-th row of the matrix $\frac{\partial}{\partial x}[J^t(x) \cdot L]$. Therefore, to calculate $\frac{\partial}{\partial x}[J^t(x) \cdot L]$, one need to apply (13) to get each its row k.

5.7. "Sliced Bread" Approach

The proposed "sliced bread" approach helps to explore the entire power flow feasibility boundary in the descriptor space and approximate it by a reasonable number of hyperplanes.

5.7.1. "Sliced Bread" Procedure in Descriptor Space

The "slice" is a cut set of the boundary obtained by varying a pair of descriptor parameters d_i and d_j while the rest of the parameters remain constant. The released parameters form a cut set plane. These parameters may be limited by some limits:

$$d_i^{\min} \le d_i \le d_i^{\max}$$
$$d_j^{\min} \le d_j \le d_j^{\max}$$

(1)

Also, within the slice, the power flow feasibility boundary could be closed (Figure 8) or open (Figure 9). Each slice is traced and approximated using the algorithm described above. The possible criteria to stop tracing the slice is are as follow:

- Acceptable distance D between the last approximating hyperplane and the first PoC in the "slice"; for instance, in Figure 8, this condition is
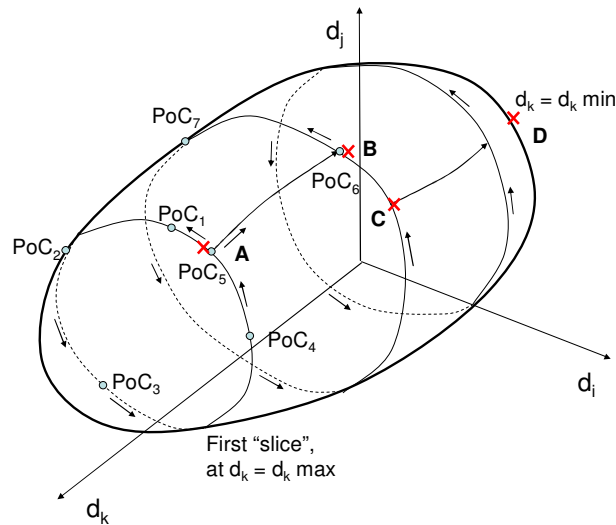
Figure 8: "Sliced bread" algorithm for the closed boundary

A – First "slice" is finished due to the "round trip" condition
A-B – Transition from the first to the second "slice"
C – Second "slice" is finished due to acceptable distance between the tangent hyperplane calculated at C and PoC$_6$
D – No more slices because p_k reaches p_{kmin}

$$r = \frac{\left\| L_5^t \cdot (PoC_5 - PoC_1) \right\|}{\left\| L_5 \right\|} \le D, \quad r \approx D$$

where L is the left eigenvector, and/or

- The "round trip" condition based on the analysis of the projections of the left eigenvectors L on the cut set plane. These projections form certain angles with the coordinate axes, for instance, with p_i:

$$\varphi_i = \arccos\left(\frac{L^t \cdot e_i}{\|L\|}\right) \tag{2}$$

E.g., for Figure 8, this angle changes from its initial value about $-90°$ to its next value $-50°$, then to $+40°$, and so on. When this angle makes a full circle so that it passes again $-90°$, this can be used as a criterion to stop tracing this particular slice.

- Cases when one of the descriptor parameters reaches its maximum or minimum value (points A and B in Figure 9).

The first slice can be selected at the maximum value of the fixed parameters, for instance, for $d_k = d_{k\max}$ in Figure 8 and Figure 9. When the "slice" is finished, the procedure goes to the next slide. For this purpose, one of the fixed parameters is temporarily released (e.g., d_k in Figure 8 and Figure 9), while one of the free parameters is temporarily fixed (e.g., d_j). The transition is implemented with the help of the same procedure that was used to approximate the "slice". The transition process ends when all fixed parameters reach their minimum values.
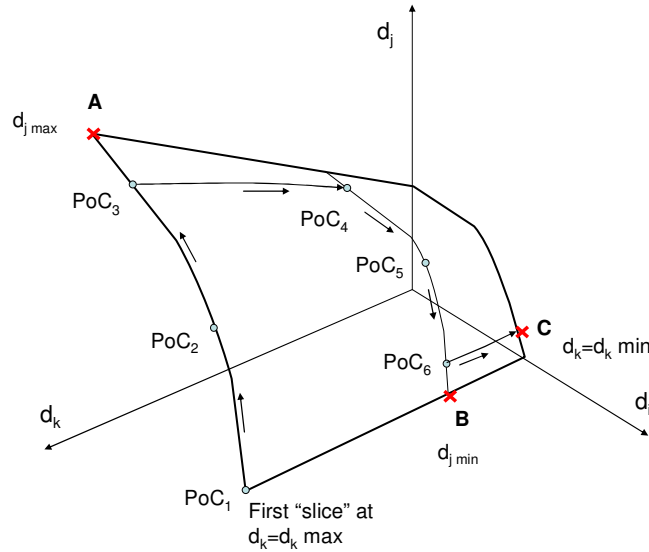

Figure 9: "Slice bread" algorithm for the open boundary

A – First "slice" is finished because $d_j = d_{jmax}$
B – Second "slice" is finished because $d_j = d_{jmin}$
C – Procedure stops because $d_k = d_{kmin}$

5.7.2.   The Algorithm in the Descriptor Space

1. Calculate the base case point in X, P and D, that is x_0, p_0 and d_0.

2. Specify an initial stress direction in D, Δd_0 using inverse mapping $\Delta p_0 = Tdir = Vector^{-1}(\Delta d_0)$.

3. Specify the first slice (d_i, d_j) in D.

4. Map the slice into P, $(p_i, p_j) = (e_i, e_j) = Plane^{-1}(d_i, d_j)$

5. Perform the parameter continuation method and direct method to determine PoC_0 in X and P. Find the left eigenvector L_0 and hyperplane H_0.

6. Map PoC_0, L_0 and H_0 back into D: $PoC_{0D} = Point(PoC_{0P})$, $L_{0D} = Vector(L_{0P})$, and $H_{0D} = Plane(H_{0P})$.

7. Initiate the Boundary Orbiting Procedure step along the slice (e_i, e_j) in P.

8. If the BOM step diverges, repeat the parameter continuation method and direct method to determine PoC_1 in X and P. Find the left eigenvector L_1 and hyperplane H_1. Go to 10.

9. Otherwise, determine PoC_1 in X and P as a result of the BOM step. Find the left eigenvector L_1 and hyperplane H_1.

10. Map PoC_1, L_1 and H_1 back into D, $PoC_{1D} = Point(PoC_{1P})$, $L_{1D} = Vector(L_{1P})$, and $H_{1D} = Plane(H_{1P})$.

11. Check the slice stop tracing criteria as described in Section 5.7.1. Go to the next slice in D and start from Step 1.

12. Otherwise map the (d_i, d_j) into P again at the new point, $(p_i, p_j) = (e_i, e_j) = Plane^{-1} (d_i, d_j)$.

5.8. Minimum Set of Hyperplanes

The objective of obtaining the minimum set of hyperplanes is to test the performance and accuracy of the proposed VSA technology, which includes the following steps:

- Selection of critical loading directions for a selected problem area
- Performance of the predictor-corrector loading procedure
- Calculation of the points of collapse and tangent hyperplanes
- Calculation of the approximating hyperplanes (secant hyperplanes)
- Evaluate the accuracy of approximation using the proposed approach and accuracy metric
- Decide on whether the proposed selection of loading directions is adequate to the study areas

5.8.1.   Procedure for Determining the Minimum Set of Hyperplanes

The following steps describe the procedure to determine the minimum set of hyperplanes:

1. Perform the predictor-corrector procedure for each selected loading direction – Sections 5.3.
2. Determine the Points of Collapse (PoC) - Section 5.4.
3. Apply inverse iterations method to calculate the left eigenvector L at the PoC – Section 5.5.
4. Calculate the tangent and secant hyperplanes – Section 5.5. To determine the required margin (d+m), use 5, 10, 15, and 20% (j=1, 2…, 4) (configurable) of the maximum loading in the most limited direction. As a result, get four sets of secant hyperplanes for each direction, corresponding to the different margin (d+m) – Figure 10 (taken from section 5.5).

The tangent hyperplane equation is:

$$L_i^t \cdot (p - PoC_i) = 0$$

The secant approximating hyperplane equation is:

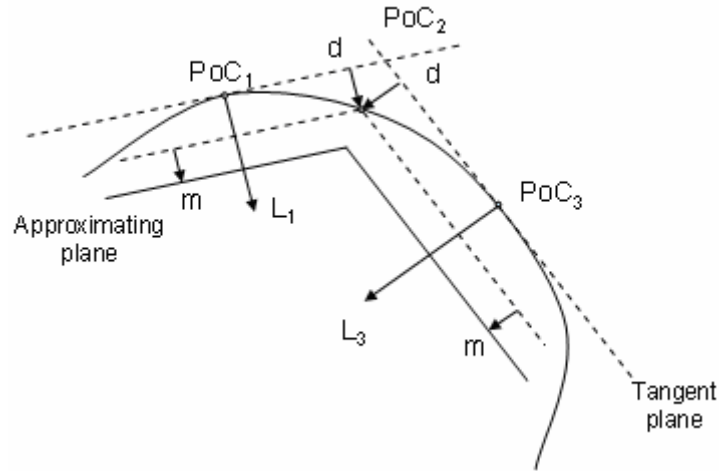$$L_i^t \cdot (p - PoC_i) = (d + m)_j$$

Figure 10: Tangent and approximating hyperplanes

5. Select 10-20 additional loading directions for each area and perform the step-by step loading procedure for the original and additional loading vectors. Evaluate the PoC_k for each direction k assuming that this is the point of divergence.

6. For each evaluated PoC_k, calculate the distance to each of the approximating hyperplanes at different margins $(d+m)_j$ using the following formula:

$$r_{ijk} = \frac{\left\| L_i^t \cdot (PoC_k - PoC_i) \right\|}{\left\| L_i \right\|} - (d+m)_j$$

7. Summarize these experimental results for each area in the following table:

Hyperplane		Loading Vector 1	Loading Vector 2	...	Loading Vector k
1	5%				
	10%				
	15%				
	20%				
2	5%				
	10%				
	15%				
	20%				
...	5%				
	10%				
	15%				
	20%				
i	5%				
	10%				
	15%				
	20%				

Distances from PoC to Hyperplanes

8. Analyze the angles between the loading vectors D_k and the left eigenvectors L_k. These angles can be calculated as follows:

12/2/07 REV 6/92008

$$\theta_{ik} = \arccos \frac{L_i^t \cdot D_k}{\|L_i\| \cdot \|D_k\|}$$

Mark all cells in the table corresponding to the case when $|\Theta_{ik}| > 60°$ (configurable). Those are the cases when hyperplane i forms a sharp angle with the loading direction k, and the distance metric r_{ijk} could be misleading. If the marked cells fill an entire column, the corresponding loading direction should be added to the original list of loading directions for which approximating hyperplanes are calculated (the entire procedure should be repeated for the added hyperplane).

9.   Analyze the columns for the loading vectors $D_1,\ldots,D_k$. Start with the j=5% cells initially. Check whether at least one distance in the column k stays within the 5% distance to the 5% approximating hyperplane. If yes, do nothing. I none of the distances are in the 5% range, check whether D_k is a direction for which an approximating hyperplane is built. If it is not, add a new approximating hyperplane to the list, but allow only 5% margin (don't calculate hyperplanes for any margins other than 5% for the newly added direction). If the analyzed direction is already the one that has an associated hyperplane, this means that the 5% accuracy is not achievable for that direction. This means that verification is not possible for that accuracy.

10.   Repeat step 9 for all other margins. If finally for each loading direction we have at least one distance within 5, 10, 15 …%, our verification is successful for the corresponding accuracy.

5.9. Descriptor Space Formulation

In this section, the formulation for descriptor variables has been discussed and the formulas for normal vector to nomogram boundaries have been derived.

Parameter space

The parameter space contains the generator and load power injections and is sometimes augmented with other states or parameters. There is a hypersurface in the parameter space corresponding to voltage collapse. Our software starts from base case parameters P_0 and given a pattern of stress and computes points on the hypersurface, the corresponding margin to voltage collapse and the normal vector to the hypersurface. It can also compute curves on the hypersurface.

One-dimensional margin to voltage collapse

We specify the pattern, or participation of all injections in a column vector *k*. Then the changes in injections are $m \times k$ where *m* is a scalar parameterization of the system stress. If the base case parameters are P_0, then the stressed system parameters parameterized by *m* is the column vector

$$P = P_0 + m \times k$$

It can be useful to normalize *k* so that *m* is expressed in some convenient way and in convenient units. For example, if the parts of *k* corresponding to generator injections are normalized to have L1 norm, then *m* measures the generation margin in L1; that is, the sum of the generation increases.

A bulk change descriptor variable *µ* is a quantity such as an area load increase or an import across a cutset. *µ* is (for a given network structure) an affine function of the parameters *P* so that

$$\mu = h \times P = h \times (P_0 + m \times k)$$

where *h* is a row vector. Note that the matrix multiplication $h \times (P_0 + m \times k)$ is the same as the dot product between h^t and $(P_0 + m \times k)$. (This formula assumes that the base case $\mu = h \times P_0$, but this can be easily generalized as needed by adding a suitable constant). *h* is a fixed row vector that can be computed from the network equations. For example, *h* for a cutset flow *µ* is computed by summing line flows for lines in the cutset as a function of injections. The scaling of *h* is chosen so that *µ* is in

convenient units such as MW of import through the cutset or MW of load. At the voltage collapse, we get:

$$\mu^* = h\ (P_0 + m^* \times k)$$

If we now assume a fixed stress direction or injection participation k, then m is also a function of μ:

$$m = \frac{\mu - h \times P_0}{h \times k}$$

Specifying μ and k now defines the system stress m and k. That is, the system stress can be specified by the amount of a bulk change of injections μ and also assuming the pattern, or participation of all injections in the column vector k.

In summary, we can formulate the one-dimensional margin to voltage collapse as follows: We make the assumption of the participation factors k. Then we can specify an amount of stress by descriptor μ and the margin to voltage collapse can be specified by the descriptor margin $\mu^* = h\ (P_0 + m^* \times k)$.

Two-dimensional voltage collapse nomogram

Here we define two bulk change descriptor variables μ and η so the descriptor variables are the column vector $d = (\mu,\eta)^T$ (superscript T indicates matrix transpose)[14]. Now h is a vector function given by the 2 $\times$ (number of parameters) matrix $h = (h_1{}^T, h_2{}^T)^T$ so that

$$d = (\mu,\eta)^T = h \times P = h\ (P_0 + m \times k)$$

The nomogram curve is given by $(\mu^*, \eta^*)^T = h\ (P_0 + m^* \times k)$ as k varies (note that m^* is a function of k). We assume that the nomogram curve is given (locally) by:

$$g(d) = g((\mu,\eta)^T) = 0$$

If we now assume two fixed stress directions or injection participations k_1 and k_2, so that

$$P = P_0 + m_1 \times k_1 + m_2 \times k_2,$$

then

$$
\begin{aligned}
d = (\mu,\eta)^T &= h\ (P_0 + m_1 \times k_1 + m_2 \times k_2) \\
&= d_0 + M\ (m_1, m_2)^T
\end{aligned}
$$

where M is the 2 x 2 matrix

$$M = [h \times k_1,\ h \times k_2]$$

Then $(m_1, m_2)^T$ and P are also affine functions of $(\mu,\eta)^T$:

$$
\begin{aligned}
(m_1, m_2)^T &= M^{-1}\ ((\mu,\eta)^T - h \times P_0) \\
P &= P_0 + (k_1, k_2) \times (m_1, m_2)^T \\
&= P_0 + (k_1, k_2) \times M^{-1} \times (d - d_0)
\end{aligned}
$$

Specifying $(\mu,\eta)^T$ and k_1 and k_2 now defines the system stress in terms of injections P. That is, the system stress can be specified by the amount of a bulk change of injections $(\mu,\eta)^T$ and also assuming the patterns, or participations of all injections in the column vectors k_1 and k_2.

---

[14] For example, for the San Diego region, we could have $(\mu,\eta)^T$ = (path 45/CFE import, SDG&E import)^T or $(\mu,\eta)^T$ = (SDG&E generation, SDG&E load)^T

In summary, we can formulate a two-dimensional margin to voltage collapse as follows: We make the assumption of the participation factor vectors k_1 and k_2. Then we can specify an amount of stress by descriptor vector $d = (\mu, \eta)^T$. The voltage collapse boundary can be specified by the curve $g(d) = 0$ in the nomogram. It is important to note the dependence of the nomogram curve on the choice of k_1 and k_2.

Relation between parameter space and nomogram normals

The descriptor parameters d considered here are affine functions of the parameter space parameters P given by

$$d = d_0 + h \times P$$

where h is a matrix.

As explained above, the nomogram curve is given by an equation

$$g(d) = 0$$

The nomogram curve has normal vector given by the row vector D_g. D_g has two components. The nomogram curve immediately induces a corresponding hypersurface in the parameter space defined by the equation

$$g(d_0 + h \times P) = 0$$

Differentiating $g(d_0 + h \times P)$ with respect to P gives the normal vector to the parameter space hypersurface

$$hyperspace\ normal = D_g \times h$$

This formula expresses the parameter space normal in terms of the nomogram curve normal and the transformation matrix h.

Now we express the nomogram curve normal in terms of the parameter space normal. Assume as above a choice of k_1 and k_2 so that

$$P = P_0 + (k_1, k_2) \times M^{-1} \times (d - d_0)$$

Let the parameter space hypersurface be given by an equation

$$f(P) = 0$$

The hypersurface has normal vector given by the row vector D_f. Then the nomogram curve is given by

$$f(P_0 + (k_1, k_2) \times M^{-1} \times (d - d_0)) = 0$$

Differentiating the left hand side with respect to d gives the normal vector to the nomogram curve

$$nomogram\ normal = D_f \times (k_1, k_2) \times M^{-1}$$

This formula expresses the nomogram normal in terms of the parameter space normal and a linear transformation.

5.10. Special Features of the RTVSA Application

The RTVSA application is based on an extensive analysis of the existing VSA approaches, by surveying the leading power system experts' opinion worldwide, and also with feedback from industrial advisors. The mismatch between the core power system reliability needs and the availability of the VSA tools was a motivation to design the following special features into the RTVSA application.

- The underlying concepts are applicable to the simple one-dimensional approach or the more complex multi-directional stressing to explore the entire voltage security region in the parameter space or in full P-Q injection space.

- The RTVSA tool has the ability of analyzing the effects of multiple transfers. There are no restrictions in distributing the source and sink over a large number of buses in geographically distant locations in the system. A non-local treatment of congestion[15] is crucial because conservatism causes costly curtailment of profitable power transfers and a suboptimal use of the transmission system.

- The RTVSA algorithm[16] in Phase 2 uses the parameter continuation method, which is one of the most reliable power flow methods capable of reaching the point of collapse on the power flow feasibility boundary. New variables called the continuation parameters are added and represents a position of a power flow operating point along some power system stress direction in the parameter space. The *predictor step* consists in an incremental moving of the power flow operating point along the state space trajectory, based on the linearization of the problem. The *corrector step*, that follows each predictor step, consists in elimination of the linearization error by balancing the power flow equations to some close point on the nonlinear trajectory.

- The RTVSA algorithm in Phase 3 use Direct methods for finding the PoC, which combines the parametric description of the system stress and the power flow singularity condition expressed with the help of the Jacobian matrix multiplied by a nonzero right or the left eigenvector that nullifies the Jacobian matrix at the collapse point. In principle, the Direct Method avoids implementing a loading procedure. There may be problems of finding the initial guesses of the state variables and the eigenvector that may be resolved by initial loading the system along the stress direction. By doing so, the initial guess of variables can be obtained. Many inaccuracies of the step-by-step loading methods that do not exactly converge to the PoC will be avoided by implementing the Direct Method. There are savings in computational expenses because of the absence of iterations even though the Direct Method solves a problem almost double in dimension to the step-by-step loading methods.

- The RTVSA algorithm determines the "right eigenvector" and the "left eigenvector" at the PoC. The weak elements are based on the right eigenvector and provide the extent to which variables participate in voltage collapse. This determines weak areas and also whether the collapse is an angle collapse. Large sensitivities of the margin to PoC indicate controllable parameters. These are represented by the left eigenvector and can be quantified for suitable corrective action by ranking the increase in margin with respect to a unit MW or MVAR in generator response.

- Sensitivity computations relate changes in data to changes in transfer capability. The uncertainty in the transfer capability due to uncertainty in the data was quantified in Phase 4 of the RTVSA algorithm. These computations revealed which data is significant in the transfer calculations.

---

[15] Congestion can be quantified more precisely as the combined effect of multiple power transfers exceeding the transfer capability of the transmission system.

[16] The RTVSA algorithm falls into the class of non-divergent power flow methods that manipulate the step size of the Newton-Raphson method. If the power flow mismatches indicate divergence, the step size is reduced until convergence occurs or the step becomes very small. A very small step size is considered to be an indicator of the point of collapse.

6. Appendix A: Hessian Metrix of Power Flow Equation

Ning Zhou, PNNL, Richland, WA 99352
10/06/2006~10/16/2006

This document describes procedures of calculating the Hessian Matrix of Power flow equations. It also discusses the vectorization procedure, which may improve the implement efficiency using Matlab. The calculation procedure of the $\frac{\partial}{\partial x}\left[J^t(x)\cdot L\right]$ is also derived.

I. Scalar Version of Second Derivatives of Power InjectionS

This section gives the identities for calculating the elements of Jacobian and Hessian matrix of power injection. Note that all the elements are in the scalar format. Thus, it may not be efficient to implement the algorithm using Matlab.

Note:

    a) Matlab is not very efficient to implement '*for*' loop.
    b) The notation used is similar to the notation used in [1] .
    c) The power injection and first derivative equations are extracted from [1].

- **Real Power Injection**

$$P_i = V_i \sum_{j=1}^{nbus} V_j \left(G_{ij}\cos\theta_{ij} + B_{ij}\sin\theta_{ij}\right)$$

First derivative w.r.t θ_i. (with fixed i)

$$\frac{\partial P_i}{\partial \theta_i} = -V_i \sum_{j=1}^{nbus} V_j\left(G_{ij}\sin\theta_{ij} - B_{ij}\cos\theta_{ij}\right) - V_i^2 B_{ii}$$

- **Second derivative wrt θ_i**

$$\frac{\partial P_i^2}{\partial \theta_i \partial \theta_i} = -V_i \sum_{j=1}^{nbus} V_j\left(G_{ij}\cos\theta_{ij} + B_{ij}\sin\theta_{ij}\right) + V_i^2 G_{ii}$$

- **Second derivative wrt θ_j (for j<>i)**

$$\frac{\partial P_i^2}{\partial \theta_i \partial \theta_j} = V_i V_j\left(G_{ij}\cos\theta_{ij} + B_{ij}\sin\theta_{ij}\right)$$

- **Second derivative wrt V_i**

$$\frac{\partial P_i^2}{\partial \theta_i \partial V_i} = -\sum_{j=1}^{nbus} V_j\left(G_{ij}\sin\theta_{ij} - B_{ij}\cos\theta_{ij}\right) - V_i B_{ii}$$

- **Second derivative wrt V_j (for j<>i)**

$$\frac{\partial P_i^2}{\partial \theta_i \partial V_j} = -V_i \left(G_{ij} \sin \theta_{ij} - B_{ij} \cos \theta_{ij} \right)$$

First derivative w.r.t θ_j (for j<>i, with fixed i and j.).

$$\frac{\partial P_i}{\partial \theta_j} = V_i V_j \left(G_{ij} \sin \theta_{ij} - B_{ij} \cos \theta_{ij} \right)$$

- **Second derivative wrt θ_i**

$$\frac{\partial P_i^2}{\partial \theta_j \partial \theta_i} = V_i V_j \left(G_{ij} \cos \theta_{ij} + B_{ij} \sin \theta_{ij} \right)$$

- **Second derivative wrt θ_j**

$$\frac{\partial P_i^2}{\partial \theta_j \partial \theta_j} = -V_i V_j \left(G_{ij} \cos \theta_{ij} + B_{ij} \sin \theta_{ij} \right)$$

- **Second derivative wrt θ_k (for k<>i, k<>j)**

$$\frac{\partial P_i^2}{\partial \theta_j \partial \theta_k} = 0$$

- **Second derivative wrt V_i**

$$\frac{\partial P_i^2}{\partial \theta_j \partial V_i} = V_j \left(G_{ij} \sin \theta_{ij} - B_{ij} \cos \theta_{ij} \right)$$

- **Second derivative wrt V_j**

$$\frac{\partial P_i^2}{\partial \theta_j \partial V_j} = V_i \left(G_{ij} \sin \theta_{ij} - B_{ij} \cos \theta_{ij} \right)$$

- **Second derivative wrt V_k (for k<>i, k<>j)**

$$\frac{\partial P_i^2}{\partial \theta_j \partial V_k} = 0$$

First derivative w.r.t V_i. (with fixed i)

$$\frac{\partial P_i}{\partial V_i} = \sum_{j=1}^{nbus} V_j \left(G_{ij} \cos \theta_{ij} + B_{ij} \sin \theta_{ij} \right) + V_i G_{ii}$$

- **Second derivative wrt θ_i**

$$\frac{\partial P_i^2}{\partial V_i \partial \theta_i} = -\sum_{j=1}^{nbus} V_j \cdot \left(G_{ij} \sin \theta_{ij} - B_{ij} \cos \theta_{ij} \right) - V_i B_{ii}$$

- **Second derivative wrt θ_j (for j<>i)**

$$\frac{\partial P_i^2}{\partial V_i \partial \theta_j} = V_j \left(G_{ij} \sin \theta_{ij} - B_{ij} \cos \theta_{ij} \right)$$

- **Second derivative wrt V_i**

$$\frac{\partial P_i^2}{\partial V_i \partial V_i} = 2 G_{ii}$$

- **Second derivative wrt V_j (for j<>i)**

$$\frac{\partial P_i^2}{\partial V_i \partial V_j} = G_{ij} \cos \theta_{ij} + B_{ij} \sin \theta_{ij}$$

First derivative w.r.t V_j. (with fixed i and j, for j<>i)

$$\frac{\partial P_i}{\partial V_j} = V_i \cdot \left(G_{ij} \cos \theta_{ij} + B_{ij} \sin \theta_{ij} \right)$$

- **Second derivative wrt θ_i**

$$\frac{\partial P_i^2}{\partial V_j \partial \theta_i} = -V_i \cdot \left(G_{ij} \sin \theta_{ij} - B_{ij} \cos \theta_{ij} \right)$$

- **Second derivative wrt θ_j**

$$\frac{\partial P_i^2}{\partial V_j \partial \theta_j} = V_i \cdot \left(G_{ij} \sin \theta_{ij} - B_{ij} \cos \theta_{ij} \right)$$

- **Second derivative wrt θ_k (for k<>i, and k<>j)**

$$\frac{\partial P_i^2}{\partial V_j \partial \theta_k} = 0$$

- **Second derivative wrt V_i**

$$\frac{\partial P_i^2}{\partial V_j \partial V_i} = G_{ij} \cos \theta_{ij} + B_{ij} \sin \theta_{ij}$$

- **Second derivative wrt V_j**

$$\frac{\partial P_i^2}{\partial V_j \partial V_j} = 0$$

- **Second derivative wrt V_k (for k<>i, and k<>j)**

$$\frac{\partial P_i^2}{\partial V_j \partial V_k} = 0$$

- Reactive Power Injection

$$Q_i = V_i \sum_{j=1}^{nbus} V_j \left(G_{ij} \sin \theta_{ij} - B_{ij} \cos \theta_{ij} \right)$$

First derivative w.r.t θ_i. (with fixed i)

$$\frac{\partial Q_i}{\partial \theta_i} = V_i \sum_{j=1}^{nbus} V_j \left(G_{ij} \cos \theta_{ij} + B_{ij} \sin \theta_{ij} \right) - V_i^2 G_{ii}$$

- **Second derivative wrt θ_i**

$$\frac{\partial Q_i^2}{\partial \theta_i \partial \theta_i} = -V_i \sum_{j=1}^{nbus} V_j \left(G_{ij} \sin \theta_{ij} - B_{ij} \cos \theta_{ij} \right) - V_i^2 B_{ii}$$

- **Second derivative wrt θ_j (for j<>i)**

$$\frac{\partial Q_i^2}{\partial \theta_i \partial \theta_j} = V_i V_j \left(G_{ij} \sin \theta_{ij} - B_{ij} \cos \theta_{ij} \right)$$

- **Second derivative wrt V_i**

$$\frac{\partial Q_i^2}{\partial \theta_i \partial V_i} = \sum_{j=1}^{nbus} V_j \left(G_{ij} \cos \theta_{ij} + B_{ij} \sin \theta_{ij} \right) - V_i G_{ii}$$

- **Second derivative wrt V_j (for j<>i)**

$$\frac{\partial Q_i^2}{\partial \theta_i \partial V_j} = V_i \left(G_{ij} \cos \theta_{ij} + B_{ij} \sin \theta_{ij} \right)$$

First derivative w.r.t θ_j. (with fixed i and j, for j<>i)

$$\frac{\partial Q_i}{\partial \theta_j} = -V_i V_j \left(G_{ij} \cos \theta_{ij} + B_{ij} \sin \theta_{ij} \right)$$

- **Second derivative wrt θ_i**

$$\frac{\partial Q_i^2}{\partial \theta_j \partial \theta_i} = V_i V_j \left(G_{ij} \sin \theta_{ij} - B_{ij} \cos \theta_{ij} \right)$$

- **Second derivative wrt θ_j**

$$\frac{\partial Q_i^2}{\partial \theta_j \partial \theta_j} = -V_i V_j \left(G_{ij} \sin \theta_{ij} - B_{ij} \cos \theta_{ij} \right)$$

- **Second derivative wrt θ_k (for k<>i, and k<>j)**

$$\frac{\partial Q_i^2}{\partial \theta_j \partial \theta_k} = 0$$

- **Second derivative wrt V_i**

$$\frac{\partial Q_i^2}{\partial \theta_j \partial V_i} = -V_j \left(G_{ij} \cos \theta_{ij} + B_{ij} \sin \theta_{ij} \right)$$

- **Second derivative wrt V_j**

$$\frac{\partial Q_i^2}{\partial \theta_j \partial V_j} = -V_i \left(G_{ij} \cos \theta_{ij} + B_{ij} \sin \theta_{ij} \right)$$

- **Second derivative wrt V_k (for k<>i, and k<>j)**

$$\frac{\partial Q_i^2}{\partial \theta_j \partial V_k} = 0$$

First derivative w.r.t V_i. (with fixed i)

$$\frac{\partial Q_i}{\partial V_i} = \sum_{j=1}^{nbus} V_j \left(G_{ij} \sin \theta_{ij} - B_{ij} \cos \theta_{ij} \right) - V_i B_{ii}$$

- **Second derivative wrt θ_i**

$$\frac{\partial Q_i^2}{\partial V_i \partial \theta_i} = \sum_{j=1}^{nbus} V_j \left(G_{ij} \cos \theta_{ij} + B_{ij} \sin \theta_{ij} \right) - V_i G_{ii}$$

- **Second derivative wrt θ_j (for j<>i)**

$$\frac{\partial Q_i^2}{\partial V_i \partial \theta_j} = -V_j \left(G_{ij} \cos \theta_{ij} + B_{ij} \sin \theta_{ij} \right)$$

- **Second derivative wrt V_i**

$$\frac{\partial Q_i^2}{\partial V_i \partial V_i} = -2 B_{ii}$$

- **Second derivative wrt V_j (for j<>i)**

$$\frac{\partial Q_i^2}{\partial V_i \partial V_j} = G_{ij} \sin \theta_{ij} - B_{ij} \cos \theta_{ij}$$

First derivative w.r.t V_j. (with fixed i and j, for j<>i)

$$\frac{\partial Q_i}{\partial V_j} = V_i \left(G_{ij} \sin \theta_{ij} - B_{ij} \cos \theta_{ij} \right)$$

- **Second derivative wrt θ_i**

$$\frac{\partial Q_i^2}{\partial V_j \partial \theta_i} = V_i \left(G_{ij} \cos \theta_{ij} + B_{ij} \sin \theta_{ij} \right)$$

- **Second derivative wrt θ_j**

$$\frac{\partial Q_i^2}{\partial V_j \partial \theta_j} = -V_i \left(G_{ij} \cos \theta_{ij} + B_{ij} \sin \theta_{ij} \right)$$

- **Second derivative wrt θ_k (for k<>i and k<>j)**

$$\frac{\partial Q_i^2}{\partial V_j \partial \theta_k} = 0$$

- **Second derivative wrt V_i**

$$\frac{\partial Q_i^2}{\partial V_j \partial V_i} = G_{ij} \sin \theta_{ij} - B_{ij} \cos \theta_{ij}$$

- **Second derivative wrt V_j**

$$\frac{\partial Q_i^2}{\partial V_j \partial V_j} = 0$$

- **Second derivative wrt V_k (for k<>i and k<>j)**

$$\frac{\partial Q_i^2}{\partial V_j \partial V_k} = 0$$

42

II Vectorized Jacobian

This section gives the vectorized Jacobian matrix. The method has been cross-validated through the comparison with the Matlab codes in [2]. Prof. DeMarco's contributions are credited in the Matlab codes. Note that the vectorized Jacobian can be implemented efficiently using Matlab.

$$S = diag(\vec{V}) \cdot conj(\vec{I})$$

$$= diag(\vec{V}) \cdot conj(Y \cdot \vec{V}) \tag{2.1}$$

$$= \begin{bmatrix} V_1 & \\ & V_2 \end{bmatrix} \cdot \begin{bmatrix} e^{j\theta_1} & \\ & e^{j\theta_2} \end{bmatrix} \cdot conj(Y) \cdot \begin{bmatrix} e^{-j\theta_1} & \\ & e^{-j\theta_2} \end{bmatrix} \cdot \begin{bmatrix} V_1 \\ V_2 \end{bmatrix}$$

2.1) Vectorized Jacobian wrt V

$$\frac{\partial S}{\partial V} = \frac{\partial}{\partial V}\left\{ diag(\vec{V}) \cdot conj(\vec{I}) \right\}$$

$$= diag(\vec{V}) \cdot \frac{\partial conj(\vec{I})}{\partial V} + diag\left[conj(\vec{I}) \right] \cdot \frac{\partial \vec{V}}{\partial V}$$

$$= diag(\vec{V}) \cdot conj(Y) \cdot \begin{bmatrix} e^{-j\theta_1} & & \\ & \ddots & \\ & & e^{-j\theta_{nbus}} \end{bmatrix} + diag[conj(Y \cdot \vec{V})] \cdot \begin{bmatrix} e^{j\theta_1} & & \\ & \ddots & \\ & & e^{j\theta_{nbus}} \end{bmatrix} \tag{2.2}$$

$$= diag(\vec{V}) \cdot conj(Y) \cdot diag\left[conj(\frac{\vec{V}}{V}) \right] + diag[conj(Y \cdot \vec{V})] \cdot diag\left[\frac{\vec{V}}{V} \right]$$

$$\frac{\partial P}{\partial V} = real\left(\frac{\partial S}{\partial V} \right) \qquad \frac{\partial Q}{\partial V} = imag\left(\frac{\partial S}{\partial V} \right) \tag{2.3}$$

2.2) Vectorized Jacobian wrt θ

$$\frac{\partial S}{\partial \theta} = \frac{\partial}{\partial \theta}\left\{ diag(\vec{V}) \cdot conj(\vec{I}) \right\}$$

$$= diag(\vec{V}) \cdot \frac{\partial conj(\vec{I})}{\partial \theta} + diag\left[conj(\vec{I}) \right] \cdot \frac{\partial \vec{V}}{\partial \theta}$$

$$= diag(\vec{V}) \cdot conj(Y) \cdot \begin{bmatrix} -jV_1 e^{-j\theta_1} & & \\ & \ddots & \\ & & -jV_{nbus} e^{-j\theta_{nbus}} \end{bmatrix} + diag[conj(Y \cdot \vec{V})] \cdot \begin{bmatrix} jV_1 e^{j\theta_1} & & \\ & \ddots & \\ & & jV_{nbus} e^{j\theta_{nbus}} \end{bmatrix}$$

$$= diag(\vec{V}) \cdot conj(Y) \cdot diag(conj(j \cdot \vec{V})) + diag[conj(Y \cdot \vec{V})] \cdot diag(j \cdot \vec{V})$$

(2.4)

$$\frac{\partial P}{\partial \theta} = real\left(\frac{\partial S}{\partial \theta} \right) \qquad \frac{\partial Q}{\partial \theta} = imag\left(\frac{\partial S}{\partial \theta} \right)$$

(2.5)

III Vectorized Hessian

Suppose that $J(x) \in R^{N \times N}$ is the "full Jacobian" matrix. Then, the *Hessian* matrix can be expressed as $\frac{\partial}{\partial x}\left[vec(J(x)) \right] \in R^{N^2 \times N}$. The vectorized Hessian matrix can be implemented more efficiently using Matlab than the scalar version.

3.1) $\quad \dfrac{\partial}{\partial \theta}\left(\dfrac{\partial S}{\partial \theta_i} \right)$

$$\frac{\partial S}{\partial \theta_i} \overset{\Delta}{=} \frac{\partial S_1}{\partial \theta_i} + \frac{\partial S_2}{\partial \theta_i} = diag(\vec{V}) \cdot conj(Y) \cdot \begin{bmatrix} 0_{(i-1)} \\ -jV_i e^{-j\theta_i} \\ 0_{(nbus-i)} \end{bmatrix} + diag[conj(Y \cdot \vec{V})] \cdot \begin{bmatrix} 0_{(i-1)} \\ jV_i e^{j\theta_i} \\ 0_{(nbus-i)} \end{bmatrix}$$

(3.1.1)

$$\frac{\partial}{\partial \theta}\left(\frac{\partial S_1}{\partial \theta_i} \right) = \left[diag(\vec{V}) \cdot conj(Y) \right] \cdot \begin{bmatrix} 0 & & \\ & -V_i e^{-j\theta_i} & \\ & & 0 \end{bmatrix} + diag\left\{ conj(Y) \cdot \begin{bmatrix} 0_{(i-1)} \\ -jV_i e^{-j\theta_i} \\ 0_{(n-i)} \end{bmatrix} \right\} \cdot \begin{bmatrix} jV_1 e^{j\theta_1} & & \\ & \ddots & \\ & & jV_{nbus} e^{j\theta_{nbus}} \end{bmatrix}$$

(3.1.2)

$$= \left[diag(\vec{V}) \cdot conj(Y) \right] \cdot \begin{bmatrix} 0 & & \\ & -V_i e^{-j\theta_i} & \\ & & 0 \end{bmatrix} + diag\left\{ diag(j\vec{V}) \cdot conj(Y) \cdot \begin{bmatrix} 0_{(i-1)} \\ -jV_i e^{-j\theta_i} \\ 0_{(n-i)} \end{bmatrix} \right\}$$

$$\frac{\partial}{\partial\theta}\left(\frac{\partial S_2}{\partial\theta_i}\right) = diag[conj(Y\cdot\vec{V})]\cdot\begin{bmatrix}0 & & \\ & -V_i e^{j\theta_i} & \\ & & 0\end{bmatrix} + diag\left\{\begin{bmatrix}0_{(i-1)} \\ jV_i e^{j\theta_i} \\ 0_{(nbus-i)}\end{bmatrix}\right\}\cdot conj(Y)\cdot\begin{bmatrix}-jV_1 e^{-j\theta_1} & & \\ & \ddots & \\ & & -jV_{nbus}e^{-j\theta_{nbus}}\end{bmatrix}$$

(3.1.3)

$$= diag\left\{diag[conj(Y\cdot\vec{V})]\cdot\begin{bmatrix}0_{(i-1)} \\ -V_i e^{j\theta_i} \\ 0_{(nbus-i)}\end{bmatrix}\right\} + diag\left\{\begin{bmatrix}0_{(i-1)} \\ jV_i e^{j\theta_i} \\ 0_{(nbus-i)}\end{bmatrix}\right\}\cdot conj(Y)\cdot diag[conj(j\vec{V})]$$

Thus,

$$\frac{\partial}{\partial\theta}\left(\frac{\partial S}{\partial\theta_i}\right) = \underbrace{[diag(\vec{V})\cdot conj(Y)]\cdot\begin{bmatrix}0 & & \\ & -V_i e^{-j\theta_i} & \\ & & 0\end{bmatrix}}_{Type\ I} + \underbrace{diag\left\{diag(\vec{V})\cdot conj(Y)\cdot\begin{bmatrix}0_{(i-1)} \\ V_i e^{-j\theta_i} \\ 0_{(n-i)}\end{bmatrix}\right\}}_{Type\ II}$$

(3.1.4)

$$+ \underbrace{diag\left\{diag[conj(Y\cdot\vec{V})]\cdot\begin{bmatrix}0_{(i-1)} \\ -V_i e^{j\theta_i} \\ 0_{(nbus-i)}\end{bmatrix}\right\}}_{Type\ II} + \underbrace{diag\left\{\begin{bmatrix}0_{(i-1)} \\ V_i e^{j\theta_i} \\ 0_{(nbus-i)}\end{bmatrix}\right\}\cdot conj(Y)\cdot diag[conj(\vec{V})]}_{Type\ III}$$

3.2) $\quad\dfrac{\partial}{\partial V}\left(\dfrac{\partial S}{\partial\theta_i}\right)$

$$\frac{\partial S}{\partial\theta_i} \overset{\Delta}{=} \frac{\partial S_1}{\partial\theta_i} + \frac{\partial S_2}{\partial\theta_i} = diag(\vec{V})\cdot conj(Y)\cdot\begin{bmatrix}0_{(i-1)} \\ -jV_i e^{-j\theta_i} \\ 0_{(nbus-i)}\end{bmatrix} + diag[conj(Y\cdot\vec{V})]\cdot\begin{bmatrix}0_{(i-1)} \\ jV_i e^{j\theta_i} \\ 0_{(nbus-i)}\end{bmatrix}$$

(3.2.1)

$$\frac{\partial}{\partial V}\left(\frac{\partial S_1}{\partial\theta_i}\right) = diag(\vec{V})\cdot conj(Y)\cdot\begin{bmatrix}0 & & \\ & -je^{-j\theta_i} & \\ & & 0\end{bmatrix} + diag\left\{conj(Y)\cdot\begin{bmatrix}0_{(i-1)} \\ -jV_i e^{-j\theta_i} \\ 0_{(nbus-i)}\end{bmatrix}\right\}\cdot\begin{bmatrix}e^{j\theta_1} & & \\ & \ddots & \\ & & e^{j\theta_{nbus-1}}\end{bmatrix}$$

(3.2.2)

$$= diag(\vec{V})\cdot conj(Y)\cdot\begin{bmatrix}0 & & \\ & -je^{-j\theta_i} & \\ & & 0\end{bmatrix} + diag\left\{\begin{bmatrix}e^{j\theta_1} & & \\ & \ddots & \\ & & e^{j\theta_{nbus-1}}\end{bmatrix}\cdot conj(Y)\cdot\begin{bmatrix}0_{(i-1)} \\ -jV_i e^{-j\theta_i} \\ 0_{(nbus-i)}\end{bmatrix}\right\}$$

$$\frac{\partial}{\partial V}\left(\frac{\partial S_2}{\partial \theta_i}\right) = diag[conj(Y \cdot \vec{V})] \cdot \begin{bmatrix} 0 & & \\ & je^{j\theta_i} & \\ & & 0 \end{bmatrix} + diag\left\{\begin{bmatrix} 0_{(i-1)} \\ jV_i e^{j\theta_i} \\ 0_{(nbus-i)} \end{bmatrix}\right\} conj(Y) \cdot \begin{bmatrix} e^{-j\theta_1} & & \\ & \ddots & \\ & & e^{-j\theta_{nbus}} \end{bmatrix} \quad (3.2.3)$$

$$\frac{\partial}{\partial V}\left(\frac{\partial S}{\partial \theta_i}\right) = \frac{\partial}{\partial V}\left(\frac{\partial S_1}{\partial \theta_i}\right) + \frac{\partial}{\partial V}\left(\frac{\partial S_2}{\partial \theta_i}\right)$$

Type I ... *Type II*

$$= diag(\vec{V}) \cdot conj(Y) \cdot \begin{bmatrix} 0 & & \\ & -je^{-j\theta_i} & \\ & & 0 \end{bmatrix} + diag\left\{\begin{bmatrix} e^{j\theta_1} & & \\ & \ddots & \\ & & e^{j\theta_{nbus}} \end{bmatrix} \cdot conj(Y) \cdot \begin{bmatrix} 0_{(i-1)} \\ -jV_i e^{-j\theta_i} \\ 0_{(nbus-i)} \end{bmatrix}\right\}$$

Type I ... *Type III*

$$+ diag[conj(Y \cdot \vec{V})] \cdot \begin{bmatrix} 0 & & \\ & je^{j\theta_i} & \\ & & 0 \end{bmatrix} + diag\left\{\begin{bmatrix} 0_{(i-1)} \\ jV_i e^{j\theta_i} \\ 0_{(nbus-i)} \end{bmatrix}\right\} conj(Y) \cdot \begin{bmatrix} e^{-j\theta_1} & & \\ & \ddots & \\ & & e^{-j\theta_{nbus}} \end{bmatrix} \quad (3.2.4)$$

3.3) $\quad \dfrac{\partial}{\partial \theta}\left(\dfrac{\partial S}{\partial V_i}\right)$

$$\frac{\partial S}{\partial V_i} \overset{\Delta}{=} \frac{\partial S_1}{\partial V_i} + \frac{\partial S_2}{\partial V_i} = \begin{bmatrix} V_1 e^{j\theta_1} & & \\ & \ddots & \\ & & V_{nbus}e^{j\theta_{nbus}} \end{bmatrix} \cdot conj(Y) \cdot \begin{bmatrix} 0_{(i-1)} \\ e^{-j\theta_i} \\ 0_{(nbus-i)} \end{bmatrix} + diag\left\{ conj(Y) \cdot \begin{bmatrix} V_1 e^{-j\theta_1} \\ \vdots \\ V_{nbus}e^{-j\theta_{nbus}} \end{bmatrix}\right\} \cdot \begin{bmatrix} 0_{(i-1)} \\ e^{j\theta_i} \\ 0_{(i-1)} \end{bmatrix} \quad (3.3.1)$$

$$\frac{\partial}{\partial \theta}\left(\frac{\partial S_1}{\partial V_i}\right) = \begin{bmatrix} V_1 e^{j\theta_1} & & \\ & \ddots & \\ & & V_{nbus}e^{j\theta_{nbus}} \end{bmatrix} \cdot conj(Y) \cdot \begin{bmatrix} 0 & & \\ & -je^{-j\theta_i} & \\ & & 0 \end{bmatrix} + diag\left\{ conj(Y) \cdot \begin{bmatrix} 0_{(i-1)} \\ e^{-j\theta_i} \\ 0_{(nbus-i)} \end{bmatrix} \right\} \cdot \begin{bmatrix} jV_1 e^{j\theta_1} & & \\ & \ddots & \\ & & jV_{nbus}e^{j\theta_{nbus}} \end{bmatrix}$$

$$= diag(\vec{V}) \cdot conj(Y) \cdot \begin{bmatrix} 0 & & \\ & -je^{-j\theta_i} & \\ & & 0 \end{bmatrix} + diag\left\{ conj(Y) \cdot \begin{bmatrix} 0_{(i-1)} \\ e^{-j\theta_i} \\ 0_{(nbus-i)} \end{bmatrix} \right\} \cdot j \cdot diag(\vec{V}) \qquad (3.3.2)$$

$$= diag(\vec{V}) \cdot conj(Y) \cdot \begin{bmatrix} 0 & & \\ & -je^{-j\theta_i} & \\ & & 0 \end{bmatrix} + diag\left\{ j \cdot diag(\vec{V}) \cdot conj(Y) \cdot \begin{bmatrix} 0_{(i-1)} \\ e^{-j\theta_i} \\ 0_{(nbus-i)} \end{bmatrix} \right\}$$

$$\frac{\partial}{\partial \theta}\left(\frac{\partial S_2}{\partial V_i}\right) = diag\left\{ conj(Y) \cdot \begin{bmatrix} V_1 e^{-j\theta_1} \\ \vdots \\ V_{nbus}e^{-j\theta_{nbus}} \end{bmatrix} \right\} \cdot \begin{bmatrix} 0 & & \\ & je^{j\theta_i} & \\ & & 0 \end{bmatrix} + diag\left\{ \begin{bmatrix} 0_{(i-1)} \\ e^{j\theta_i} \\ 0_{(i-1)} \end{bmatrix} \right\} \cdot conj(Y) \cdot (-j) \cdot diag\left\{ \begin{bmatrix} V_1 e^{-j\theta_1} \\ \vdots \\ V_{nbus}e^{-j\theta_{nbus}} \end{bmatrix} \right\} \qquad (3.3.3)$$

$$= diag\left\{ diag\left[conj(Y \cdot \vec{V}) \right] \cdot \begin{bmatrix} 0 \\ je^{j\theta_i} \\ 0 \end{bmatrix} \right\} + diag\left\{ \begin{bmatrix} 0_{(i-1)} \\ e^{j\theta_i} \\ 0_{(i-1)} \end{bmatrix} \right\} \cdot conj\left[Y \cdot j \cdot diag(\vec{V}) \right]$$

$$\frac{\partial}{\partial \theta}\left(\frac{\partial S}{\partial V_i}\right) \overset{\Delta}{=} \frac{\partial}{\partial \theta}\left(\frac{\partial S_1}{\partial V_i}\right) + \frac{\partial}{\partial \theta}\left(\frac{\partial S_2}{\partial V_i}\right)$$

$$= \underbrace{diag(\vec{V}) \cdot conj(Y) \cdot \begin{bmatrix} 0 & & \\ & -je^{-j\theta_i} & \\ & & 0 \end{bmatrix}}_{\text{Type I}} + \underbrace{diag\left\{ j \cdot diag(\vec{V}) \cdot conj(Y) \cdot \begin{bmatrix} 0_{(i-1)} \\ e^{-j\theta_i} \\ 0_{(nbus-i)} \end{bmatrix} \right\}}_{\text{Type II}} \qquad (3.3.4)$$

$$+ \underbrace{diag\left\{ diag\left[conj(Y \cdot \vec{V}) \right] \cdot \begin{bmatrix} 0 \\ je^{j\theta_i} \\ 0 \end{bmatrix} \right\}}_{\text{Type II}} + \underbrace{diag\left\{ \begin{bmatrix} 0_{(i-1)} \\ e^{j\theta_i} \\ 0_{(i-1)} \end{bmatrix} \right\} \cdot conj\left[Y \cdot j \cdot diag(\vec{V}) \right]}_{\text{Type III}}$$

3.4) $\quad \dfrac{\partial}{\partial V}\left(\dfrac{\partial S}{\partial V_i}\right)$

$$\frac{\partial S}{\partial V_i} \overset{\Delta}{=} \frac{\partial S_1}{\partial V_i} + \frac{\partial S_2}{\partial V_i} = diag(\vec{V}) \cdot conj(Y) \cdot \begin{bmatrix} 0_{(i-1)} \\ e^{-j\theta_i} \\ 0_{(nbus-i)} \end{bmatrix} + diag[conj(Y \cdot \vec{V})] \cdot \begin{bmatrix} 0_{(i-1)} \\ e^{j\theta_i} \\ 0_{(i-1)} \end{bmatrix} \tag{3.4.1}$$

$$\frac{\partial}{\partial V}\left(\frac{\partial S_1}{\partial V_i}\right)$$

$$= diag\left\{ conj(Y) \cdot \begin{bmatrix} \vec{0}_{i-1} \\ e^{-j\theta_i} \\ \vec{0}_{nbus-i} \end{bmatrix} \right\} \cdot \begin{bmatrix} e^{j\theta_1} & & \\ & \ddots & \\ & & e^{j\theta_{nbus}} \end{bmatrix} \tag{3.4.2}$$

$$= diag\left\{ \begin{bmatrix} e^{j\theta_1} & & \\ & \ddots & \\ & & e^{j\theta_{nbus}} \end{bmatrix} \cdot conj(Y) \cdot \begin{bmatrix} 0_{(i-1)} \\ e^{-j\theta_i} \\ 0_{(nbus-i)} \end{bmatrix} \right\}$$

$$\frac{\partial}{\partial V}\left(\frac{\partial S_2}{\partial V_i}\right) = diag\begin{bmatrix} 0_{(i-1)} \\ e^{j\theta_i} \\ 0_{(nbus-i)} \end{bmatrix} \cdot conj(Y) \cdot \begin{bmatrix} e^{-j\theta_1} & & \\ & \ddots & \\ & & e^{-j\theta_{nbus}} \end{bmatrix} \tag{3.4.3}$$

Thus,

$$\frac{\partial}{\partial V}\left(\frac{\partial S}{\partial V_i}\right) \overset{\Delta}{=} \frac{\partial}{\partial V}\left(\frac{\partial S_1}{\partial V_i}\right) + \frac{\partial}{\partial V}\left(\frac{\partial S_2}{\partial V_i}\right)$$

$$= \underbrace{diag\left\{ \begin{bmatrix} e^{j\theta_1} & & \\ & \ddots & \\ & & e^{j\theta_{nbus}} \end{bmatrix} \cdot conj(Y) \cdot \begin{bmatrix} 0_{(i-1)} \\ e^{-j\theta_i} \\ 0_{(nbus-i)} \end{bmatrix} \right\}}_{Type\ II} + \underbrace{diag\begin{bmatrix} 0_{(i-1)} \\ e^{j\theta_i} \\ 0_{(nbus-i)} \end{bmatrix} \cdot conj(Y) \cdot \begin{bmatrix} e^{-j\theta_1} & & \\ & \ddots & \\ & & e^{-j\theta_{nbus}} \end{bmatrix}}_{Type\ III} \tag{3.4.4}$$

IV. Derivative of Transposed Jacobian Multiplied by Left EigenVector

To implement the transposed direct method, we need to calculate $\frac{\partial}{\partial x}\left[J^t(x) \cdot L\right]$ as described in [3]. An approximate expression for calculating $\frac{\partial}{\partial x}\left[J^t(x) \cdot L\right]$ is described in [3]. This section describes a procedure using the Hessian Matrix, which is an accurate expression. Also, the implementing efficiency using Matlab is also considered.

4.1) Basic formula

$$\frac{\partial}{\partial x}\left[J^t(x) \cdot L\right] = \frac{\partial}{\partial x}\left[L^t \cdot J(x)\right] = (I_p \otimes L^t)\frac{\partial}{\partial x}\left[vec(J(x))\right] = \begin{bmatrix} L^t \frac{\partial}{\partial x}[J_{*1}(x)] \\ L^t \frac{\partial}{\partial x}[J_{*2}(x)] \\ \vdots \\ L^t \frac{\partial}{\partial x}[J_{*N}(x)] \end{bmatrix} = \begin{bmatrix} L^t \frac{\partial}{\partial x}[\frac{\partial}{\partial x_1}F(x)] \\ L^t \frac{\partial}{\partial x}[\frac{\partial}{\partial x_2}F(x)] \\ \vdots \\ L^t \frac{\partial}{\partial x}[\frac{\partial}{\partial x_N}F(x)] \end{bmatrix}$$

$$\begin{bmatrix} L_{P_1} & L_{P_2} & L_{Q_1} & L_{Q_2} & L_{\Delta\theta_{RB}} & L_{\Delta V_{PV}} \end{bmatrix} \cdot \begin{matrix} \theta_1 & \theta_2 & V_1 & V_2 & \beta_1 & Q_{PV} \\ \begin{bmatrix} \frac{\partial P_1}{\partial \theta_1} \\ \frac{\partial P_2}{\partial \theta_1} \\ \frac{\partial Q_1}{\partial \theta_1} \\ \frac{\partial Q_2}{\partial \theta_1} \\ \frac{\partial \Delta\theta_{RB}}{\partial \theta_1} \\ \frac{\partial \Delta V_{PV}}{\partial \theta_1} \end{bmatrix} & \end{matrix} \qquad (4.1)$$

Notation:

$F(x)$ is defined in (1.3) of [4]

N=2*nbus+1+n_{pv}

$$x = [\theta; \quad V; \quad \beta_1; \quad Q_{pv}] \in R^{N \times 1}$$

$L \in R^{N \times 1}$ is the left eigen-vector of the Jacobian *matrix*.

$J(x) \in R^{N \times N}$ is the "full Jacobian" matrix

Vec(*) operator vectorizes a matrix by stacking its columns. For example,

$$vec\left(\begin{bmatrix} 1 & 2 \\ 3 & 4 \end{bmatrix}\right) = \begin{bmatrix} 1 \\ 3 \\ 2 \\ 4 \end{bmatrix}$$

$\frac{\partial}{\partial x}\left[vec(J(x))\right] \in R^{N^2 \times N}$ is the Hessian *matrix*.

Kronecker product: $A \otimes B \overset{\Delta}{=} \begin{bmatrix} A_{11}B & A_{12}B & \cdots & A_{1n}B \\ A_{21}B & A_{22}B & \cdots & A_{2n}B \\ \vdots & \vdots & \ddots & \vdots \\ A_{m1}B & A_{m2}B & \cdots & A_{mn}B \end{bmatrix}$

4.2) To improve coding efficiency

Combined with (4.1), the matrix multiplications described in [section III: Vectorized Hessian] can be implement more efficiently considering their structure features.
There are three types of structure:

4.2.1) Type I

Definition:

$$\left[diag(\vec{V}) \cdot conj(Y)\right] \cdot \begin{bmatrix} 0 & & \\ & -V_i e^{-j\theta_i} & \\ & & 0 \end{bmatrix} \Rightarrow A \cdot \begin{bmatrix} 0 & & \\ & k_i & \\ & & 0 \end{bmatrix} \tag{4.2}$$

Left eigen-vector multiplication:

$$\begin{bmatrix} L_P \\ L_Q \end{bmatrix}^t \cdot \begin{bmatrix} real\left(A \cdot \begin{bmatrix} 0 \\ & k_i \\ & & 0 \end{bmatrix} \right) \\ imag\left(A \cdot \begin{bmatrix} 0 \\ & k_i \\ & & 0 \end{bmatrix} \right) \end{bmatrix} = \begin{bmatrix} L_P^t & L_Q^t \end{bmatrix} \cdot \begin{bmatrix} real\begin{bmatrix} 0 & k_i A_{*i} & 0 \end{bmatrix} \\ imag\begin{bmatrix} 0 & k_i A_{*i} & 0 \end{bmatrix} \end{bmatrix} = \begin{bmatrix} 0 & real(k_i L_p^t A_{*i}) + imag(k_i L_Q^t A_{*i}) & 0 \end{bmatrix} \tag{4.3}$$

, where A_{*i} stands for the ith column of A matrix .

Matrix format

Let: $B \stackrel{\Delta}{=} A \cdot \begin{bmatrix} k_1 \\ & k_i \\ & & k_n \end{bmatrix}$

$$diag\left\{ \begin{bmatrix} L_P \\ L_Q \end{bmatrix}^t \cdot \begin{bmatrix} real(B) \\ imag(B) \end{bmatrix} \right\}$$

$$= diag\left\{ \begin{bmatrix} L_P \\ L_Q \end{bmatrix}^t \cdot \begin{bmatrix} real\left(A \cdot \begin{bmatrix} k_1 \\ & k_i \\ & & k_n \end{bmatrix} \right) \\ imag\left(A \cdot \begin{bmatrix} k_1 \\ & k_i \\ & & k_n \end{bmatrix} \right) \end{bmatrix} \right\} = diag\left\{ \begin{bmatrix} L_P^t & L_Q^t \end{bmatrix} \cdot \begin{bmatrix} real\left(\begin{bmatrix} k_1 A_{*1} & k_i A_{*i} & k_n A_{*n} \end{bmatrix} \right) \\ imag\left(\begin{bmatrix} k_1 A_{*1} & k_i A_{*i} & k_n A_{*n} \end{bmatrix} \right) \end{bmatrix} \right\}$$

$$= diag\left\{ \begin{bmatrix} real(k_1 L_p^t A_{*1}) + imag(k_1 L_Q^t A_{*1}) & real(k_i L_p^t A_{*i}) + imag(k_i L_Q^t A_{*i}) & real(k_n L_p^t A_{*n}) + imag(k_n L_Q^t A_{*n}) \end{bmatrix} \right\}$$

$$\tag{4.4}$$

Notice that each row of (4.4) is same as (4.3). Thus (4.4) can be used to calculate the (4.3) in matrix format

4.2.2) Type II

Definition:

$$diag\left\{diag(j\vec{V})\cdot conj(Y)\cdot\begin{bmatrix}0_{(i-1)}\\-jV_ie^{-j\theta_i}\\0_{(n-i)}\end{bmatrix}\right\}\Rightarrow diag\left\{A\cdot\begin{bmatrix}0\\k_i\\0\end{bmatrix}\right\}$$ (4.5)

Left eigen-vector multiplication:

$$\begin{bmatrix}L_P\\L_Q\end{bmatrix}^t\cdot\begin{bmatrix}real\left(diag\left\{A\cdot\begin{bmatrix}0\\k_i\\0\end{bmatrix}\right\}\right)\\imag\left(diag\left\{A\cdot\begin{bmatrix}0\\k_i\\0\end{bmatrix}\right\}\right)\end{bmatrix}=\begin{bmatrix}L_P^t & L_Q^t\end{bmatrix}\cdot\begin{bmatrix}diag\{real(k_iA_{*i})\}\\diag\{imag(k_iA_{*i})\}\end{bmatrix}$$

$$=L_P^t diag\{real(k_iA_{*i})\}+L_Q^t diag\{imag(k_iA_{*i})\}$$

(4.6)

, where A_{*i} stands for the ith column of A matrix .

Matrix format

$$B\overset{\Delta}{=}A\cdot\begin{bmatrix}k_1 & & \\ & k_i & \\ & & k_n\end{bmatrix}$$

$$[real(B)^t \quad imag(B)^t] \cdot \begin{bmatrix} diag(L_P) \\ diag(L_Q) \end{bmatrix}$$

$$= \left[real\left(A \cdot \begin{bmatrix} k_1 & & \\ & k_i & \\ & & k_n \end{bmatrix} \right)^t \quad imag\left(A \cdot \begin{bmatrix} k_1 & & \\ & k_i & \\ & & k_n \end{bmatrix} \right)^t \right] \cdot \begin{bmatrix} diag(L_P) \\ diag(L_Q) \end{bmatrix}$$

$$= \left\{ \begin{bmatrix} diag(L_P) \\ diag(L_Q) \end{bmatrix}^t \cdot \begin{bmatrix} real\left(A \cdot \begin{bmatrix} k_1 & & \\ & k_i & \\ & & k_n \end{bmatrix} \right) \\ imag\left(A \cdot \begin{bmatrix} k_1 & & \\ & k_i & \\ & & k_n \end{bmatrix} \right) \end{bmatrix} \right\} = \left\{ [diag(L_P) \quad diag(L_Q)] \cdot \begin{bmatrix} real([k_1 A_{*1} \quad k_i A_{*i} \quad k_n A_{*n}]) \\ imag([k_1 A_{*1} \quad k_i A_{*i} \quad k_n A_{*n}]) \end{bmatrix} \right\}^t$$

$$= [real(k_1 diag(L_P) \cdot A_{*1}) + imag(k_1 diag(L_Q) \cdot A_{*1}) \quad real(k_i diag(L_P) \cdot A_{*i}) + imag(k_i diag(L_Q) \cdot A_{*i}) \quad real(k_n diag(L_P) \cdot A_{*n}) + imag(k_n diag(L_Q) \cdot A_{*n})]^t$$

$$= [real(diag(k_1 A_{*1}) \cdot L_P) + imag(diag(k_1 A_{*1}) \cdot L_Q) \quad real(diag(k_i A_{*i}) \cdot L_P) + imag(diag(k_i A_{*i}) \cdot L_Q) \quad real(diag(k_n A_{*n}) \cdot L_P) + imag(diag(k_n A_{*n}) \cdot L_Q)]^t$$

$$= \begin{bmatrix} real(L_P^t \cdot diag(k_1 A_{*1})) + imag(L_Q^t \cdot diag(k_1 A_{*1})) \\ real(L_P^t \cdot diag(k_i A_{*i})) + imag(L_Q^t \cdot diag(k_i A_{*i})) \\ real(L_P^t \cdot diag(k_n A_{*n})) + imag(L_Q^t \cdot diag(k_n A_{*n})) \end{bmatrix}$$

$$= \begin{bmatrix} L_P^t \cdot real(diag(k_1 A_{*1})) + L_Q^t \cdot imag(diag(k_1 A_{*1})) \\ L_P^t \cdot real(diag(k_i A_{*i})) + L_Q^t \cdot imag(diag(k_i A_{*i})) \\ L_P^t \cdot real(diag(k_n A_{*n})) + L_Q^t \cdot imag(diag(k_n A_{*n})) \end{bmatrix}$$

(4.7)

Notice that each row of (4.7) is same as (4.6). Thus (4.7) can be used to calculate the (4.6) in matrix format.

4.2.2) Type III

Definition:

$$diag\left\{\begin{bmatrix} 0_{(i-1)} \\ jV_i e^{j\theta_i} \\ 0_{(nbus-i)} \end{bmatrix}\right\} \cdot conj(Y) \cdot diag\left[conj(j\vec{V})\right] \Rightarrow \begin{bmatrix} 0 \\ & k_i \\ & & 0 \end{bmatrix} A \quad (4.8)$$

Left eigen-vector multiplication:

$$\begin{bmatrix} L_P \\ L_Q \end{bmatrix}^t \cdot \begin{bmatrix} real\left(\begin{bmatrix} 0 \\ & k_i \\ & & 0 \end{bmatrix} A\right) \\ imag\left(\begin{bmatrix} 0 \\ & k_i \\ & & 0 \end{bmatrix} A\right) \end{bmatrix} = \begin{bmatrix} L_P^t & L_Q^t \end{bmatrix} \begin{bmatrix} real\left(\begin{bmatrix} 0 \\ k_i A_{i*} \\ 0 \end{bmatrix}\right) \\ imag\left(\begin{bmatrix} 0 \\ k_i A_{i*} \\ 0 \end{bmatrix}\right) \end{bmatrix} = L_{P_i} \cdot real(k_i A_{i*}) + L_{Q_i} \cdot imag(k_i A_{i*}) \quad (4.9)$$

, where A_{i*} stands for the ith row of A matrix .

Matrix format

Let: $B \overset{\Delta}{=} \begin{bmatrix} k_1 \\ & k_i \\ & & k_n \end{bmatrix} \cdot A$

$$\begin{bmatrix} diag(L_P) \\ diag(L_Q) \end{bmatrix}^t \cdot \begin{bmatrix} real(B) \\ imag(B) \end{bmatrix}$$

$$= \begin{bmatrix} diag(L_P) \\ diag(L_Q) \end{bmatrix}^t \cdot \begin{bmatrix} real\left(\begin{bmatrix} k_1 & & \\ & k_i & \\ & & k_n \end{bmatrix} \cdot A\right) \\ imag\left(\begin{bmatrix} k_1 & & \\ & k_i & \\ & & k_n \end{bmatrix} \cdot A\right) \end{bmatrix} = \begin{bmatrix} diag(L_P) & diag(L_Q) \end{bmatrix} \cdot \begin{bmatrix} real\begin{pmatrix} k_1 A_{1*} \\ k_i A_{i*} \\ k_n A_{n*} \end{pmatrix} \\ imag\begin{pmatrix} k_1 A_{1*} \\ k_i A_{i*} \\ k_n A_{n*} \end{pmatrix} \end{bmatrix}$$

$$= diag(L_P) \cdot real\begin{pmatrix} k_1 A_{1*} \\ k_i A_{i*} \\ k_n A_{n*} \end{pmatrix} + diag(L_Q) \cdot imag\begin{pmatrix} k_1 A_{1*} \\ k_i A_{i*} \\ k_n A_{n*} \end{pmatrix}$$

$$= \begin{bmatrix} L_{P_1} \cdot real(k_1 A_{1*}) + L_{Q_1} \cdot imag(k_1 A_{1*}) \\ L_{P_i} \cdot real(k_i A_{i*}) + L_{Q_i} \cdot imag(k_i A_{i*}) \\ L_{P_n} \cdot real(k_n A_{n*}) + L_{Q_n} \cdot imag(k_n A_{n*}) \end{bmatrix} \tag{4.10}$$

Notice that each row of (4.10) is same as (4.9). Thus (4.10) can be used to calculate the (4.9) in matrix format.

V. Notation and Matrix Identity:

5.1) Notation:

$$\theta_{ij} = \theta_i - \theta_j$$

$$Y_{ij} = G_{ij} + jB_{ij} \quad (2.4)$$

$$diag(\vec{V}) = \begin{bmatrix} V_1 e^{j\theta_1} & & \\ & \ddots & \\ & & V_{nbus} e^{j\theta_{nbus}} \end{bmatrix}$$

$$\vec{V} = \begin{bmatrix} V_1 e^{j\theta_1} \\ \vdots \\ V_{nbus} e^{j\theta_{nbus}} \end{bmatrix}$$

5.2) Basic Identity:

$$\sin' x = \cos x \qquad \cos' x = -\sin x$$

$$S = diag(\vec{V}) \cdot conj(\vec{I}) \qquad \qquad S = diag(conj(\vec{I})) \cdot (\vec{V})$$
$$\qquad = diag(\vec{V}) \cdot conj(Y \cdot \vec{V}) \qquad \text{or} \qquad \qquad = diag(conj(Y \cdot \vec{V})) \cdot \vec{V}$$

$$diag(f) \cdot g = diag(g) \cdot f$$

$$\frac{\partial A f(x)}{\partial x} = A \frac{\partial f(x)}{\partial x}$$

$$diag(f) \cdot diag(g)$$
$$= diag\{diag(f) \cdot g\}$$
$$= diag\{diag(g) \cdot f\}$$

$$\frac{\partial}{\partial x}\{diag[f(x)]\cdot g(x)\} = \frac{\partial}{\partial x}\{diag[g(x)]\cdot f(x)\}$$

$$= diag[f(x)]\cdot \frac{\partial}{\partial x}\{g(x)\} + diag[g(x)]\cdot \frac{\partial}{\partial x}\{f(x)\}$$

$$diag(\vec{V}) = \begin{bmatrix} V_1 & \\ & V_2 \end{bmatrix} \cdot \begin{bmatrix} e^{j\theta_1} & \\ & e^{j\theta_2} \end{bmatrix} = \begin{bmatrix} e^{j\theta_1} & \\ & e^{j\theta_2} \end{bmatrix} \cdot \begin{bmatrix} V_1 & \\ & V_2 \end{bmatrix}$$

$$\vec{V} = \begin{bmatrix} e^{j\theta_1} & \\ & e^{j\theta_2} \end{bmatrix} \cdot \begin{bmatrix} V_1 \\ V_2 \end{bmatrix} = \begin{bmatrix} V_1 & \\ & V_2 \end{bmatrix} \cdot \begin{bmatrix} e^{-j\theta_1} \\ e^{-j\theta_2} \end{bmatrix}$$

$$D[f(x)g(x)] = (g(x)^\top \otimes I_m)f'(x) + (I_p \otimes f(x))g'(x).$$

Reference

[1] Ali Abur, *Power System State Estimation Theory and implementation,* Marcel Dekker, Inc, 2004
[2] PSERC's matlab code of Predictor-Corrector Algorithm.
[3] Yuri Makarov, Stability Boundary Orbiting Procedure, Sept. 2006.
[4] Yuri Makarov, Understanding of Transition from PSERC Predictor-Corrector Algorithm to Direct Method, July 28, 2006

7. REFERENCES

[1] P. Kundur, Power System Stability and Control, New York: McGraw-Hill, 1994.

[2] S. Lindahl, "Case studies of recent blackouts", CRIS International Workshop on Power System Blackouts ~ Causes, Analyses, and Countermeasures, Lund, Sweden, May 3, 2004.

[3] Final Report on the August 14, 2003 Blackout in the United States and Canada: Causes and Recommendations, U.S. – Canada Power System Outage Task Force, April 5, 2004. Available online at http://www.nerc.com/~filez/blackout.html

[4] G. Doorman, G. Kjølle, K. Uhlen, E. S. Huse, and N. Flatabø, "Vulnerability of the Nordic Power System", Report to the Nordic Council of Ministers, SINTEF Energy Research, May 2004. Available online at http://sparky.harvard.edu/hepg/Papers/Doorman.vul.nordic.system.0504.pdf

[5] A. Kurita and T. Sakurai, "The Power System Failure on July 23, 1987 in Tokyo", in Proceedings of the 27th Conference on Decision and Control, December 1988.

[6] G.C. Bullock, "Cascading Voltage Collapse in West Tennessee, August 22, 1987", Georgia Institute of Technology 44th Annual Protective Relaying Conference, May 2--4 1990.

[7] "The Electric Power Outages in the Western United States, July 2-3, 1996", DOE Report to the President, August 2, 1996. Available online at ftp://www.nerc.com/pub/sys/all_updl/docs/pubs/doerept.pdf

[8] "Western Systems Coordinating Council Disturbance Report for the Power System Outage that Occurred on the Western Interconnection on August 10, 1996", October 18, 1996. Available online at ftp://www.nerc.com/pub/sys/all_updl/docs/pubs/AUG10FIN.pdf

[9] "California ISO System Disturbance Report: December 8, 1998 - San Francisco Area". Available online at http://www.caiso.com/docs/1999/03/31/1999033116341717931.pdf

[10] N. Dizdarevic, M. Majstrovic, S. Cudjic Coko, N. Mandic, and J. Bonovic, "Causes, Analyses and Countermeasures with Respect to Blackout in Croatia on January 12, 2003", CRIS International Workshop on Power System Blackouts ~ Causes, Analyses, and Countermeasures, Lund, Sweden, May 3, 2004.

[11] "Technical Analysis of the August 14, 2003, Blackout: What Happened, Why, and What Did We Learn?", Report to the NERC Board of Trustees by the NERC Steering Group, July 13, 2004. Available online at ftp://www.nerc.com/pub/sys/all_updl/docs/blackout/ NERC_Final_Blackout_Report_07_13_04.pdf

[12] "Power failure in Eastern Denmark and Southern Sweden on 23 September 2003", Final report on the course of events, Ekraft System, November 4, 2003. Available online at http://www.elkraft-system.dk

[13] "The Black-Out In Southern Sweden and Eastern Denmark", 23 September, 2003, Preliminary Report, PM 2003-10-02, Svenska Kraftnät. Available at http://www.svk.se/upload/3195/Disturbance_Sweden_DenmarkSept23.pdf

[14] "Interim Report of the Investigation Committee on the 28 September 2003 Blackout in Italy", Press Release, Union for the Coordination of Transmission of Electricity UCTE, Brussels, Belgium, October 3, 2003. Available online at http://www.energie-schweiz.ch/imperia/md/content/medienmitteilungen/mm06-122003/82.pdf

[15] "Black-Out: The Events Of 28 September 2003", Press Release, Gestore Rete Transmissione Nazionale, Italy, October 1, 2003. Available online at http://www.grtn.it/eng/documentinewsstatiche/blackout28set03.pdf

[16] C, Vournas, "Technical Summary on the Athens and Southern Greece Blackout of July 12, 2004". Available online at http://www.pserc.org/Greece_Outage_Summary.pdf

[17] Отчет по расследованию аварии в ЕЭС России, происшедшей 25.05.2005. Председатель комиссии по расследованию аварии В.К.Паули, 18 июня 2005г. [Report on failure inquiry in UES of Russia that took place at May 25,2005 – in Russian]. Available online at: http://www.mosenergo.ru/download/r410_account.zip.

[18] "Voltage Stability of Power Systems: Concepts, Analytical Tools, and Industry Experience", IEEE Special Publication90TH0358-2-PWR, 1990.

[19] "Modeling of Voltage Collapse Including Dynamic Phenomena", CIGRE Task Force 38-02-10, 1993.

[20] P. W. Sauer, K. Tomsovic, J. Dagle, S. Widergren, T. Nguyen, and L. Schienbein, "Integrated Security Analysis", Final Report, CERTS, July 2004. Available online at http://certs.lbl.gov/CERTS_P_RealTime.html

[21] "Memorandum on the Development and the Reasons of the East Coast US Blackout on August 14, 2003", Department of Relay Protection and Automatics, SO-CDA, September 10, 2003 – in Russian.

[22] S. Vakhterov, "It Was Possible to Avoid the Blackout", Power Market, No. 1, 2004. – In Russian.

[23] Y. V. Makarov, V. I. Reshetov, V. A. Stroev, and N. I. Voropai, "Blackout Prevention in the United States, Europe and Russia", Proceedings of the IEEE - Special Issue on Power Technology & Policy "Forty years after the 1965 Blackout", Vol. 93, No. 11, November 2005, pp. 1942-1955 (Invited paper).

[24] "Voltage Stability Criteria, Undervoltage Load Shedding Strategy, and Reactive Power Reserve Monitoring Methodology", Final Report, Reactive Power Reserve Work Group, Western Electricity Coordinating Council, May 1998. Available online at http://www.wecc.biz/modules.php?op=modload&name=Downloads&file=index&req=getit&lid=1038

[25] T. Van Cutsem and R. Mailhot, "Validation of a Fast Voltage Stability Analysis Method on the Hydro-Quebec System", IEEE Transactions on Power Systems, Vol. 12, No. 1, pp. 282-292, February 1997.

[26] B. Gao, G. K. Morrison, and P. Kundur, "Voltage Stability Evaluation Using Modal Analysis", IEEE Trans. on Power Systems, Vol. 7, No. 4, November 1992, pp. 1529-1542.

[27] "Reliability Criteria", Western Electricity Coordinating Council, April 2005. Available online at http://www.wecc.biz/modules.php?op=modload&name=Downloads&file=index&req=getit&lid=1029

[28] C. W. Taylor, Power System Voltage Stability. New York: McGraw-Hill, 1994.

[29] T.J.E Miller, Editor, Reactive Power Control in Electric Systems. New York: John Wiley & Sons, 1982

[30] H. K Clark, "More attention to reactive [power] and voltage will present opportunities to improve grid reliability", DOE Blackout forum, December 22, 2003. Available online at http://www.electricity.doe.gov/govforums/view_thread2.cfm?post_id=186.

[31] T. Van Cutsem, I. Dobson (Editor), C. DeMarco, D. Hill, I. Hiskens, T. Overbye, M. Venkatasubramanian, C. Vournas, Basic Theoretical Concepts, Chapter 2, IEEE Voltage Stability Work Group Report, April 1998. Available online at http://eceserv0.ece.wisc.edu/~dobson/WG/.

[32] B.M. Weedy and B.R. Cox, "Voltage stability of radial power links", Proc. IEEE, Vol.115, pp. 528-536, April 1968.

[33] P. M. Anderson and A. A. Fouad. Power System Control and Stability, IEEE Press, New York 1994.

[34] A. M. Lyapunov, The General Problem of the Stability of Motion, London, Washington DC, Tayor & Francis, 1992.

[35] R. Seydel, From Equilibrium to Chaos: Practical Bifurcation and Stability Analysis, Springer-Verlag, New York, 1994.

[36] S. Strogatz, Nonlinear Dynamics and Chaos: with Applications in Physics, Biology, Chemistry, and Engineering, Addison-Wesley, Reading MA, 1994.

[37] Thompson, J.M.T., Stewart, H.B., Nonlinear Dynamics and Chaos: Geometrical Methods for Engineers and Scientists, John Wiley, New York, 1986.

[38] E.H. Abed, P.P. Varaiya, "Nonlinear Oscillations in Power Systems", International Journal of Electric Energy and Power Systems, vol. 6, no. 1, January 1984, pp. 37-43.

[39] C.-W. Tan, M. Varghese, P. Varaiya, F.F. Wu, "Bifurcation, Chaos, and Voltage Collapse in Power Systems", Proceedings of the IEEE, Special issue on nonlinear phenomena in power systems, November 1995, vol. 83, no. 11, pp. 1484-1539.

[40] V. Ajjarapu and B. Lee, "Bibliography on Voltage stability", Available online at http://www.ee.iastate.edu/~venkatar/Biblio/biblio.html#Group5.

[41] V. A. Venikov, V. A. Stroev, V. I. Idelchick, and V. I. Tarasov, "Estimation of electric power system steady-state stability in load flow calculation", IEEE Trans. on Power Apparatus and Systems, Vol. PAS-94, pp.1034 - 1041, May/June 1975.

[42] R. C. Hardiman, M. Kumbale, and Y. V. Makarov, "An Advanced Tool for Analyzing Multiple Cascading Failures", Proceedings of the 8th International Conference on Probabilistic Methods Applied to Power Systems, Iowa State University, Ames, Iowa, September 12-16, 2004.

[43] I. Dobson, "The Irrelevance of Load Dynamics for the Loading Margin to Voltage Collapse and its Sensitivities", in L. H. Fink, Editor, Bulk power system voltage phenomena III, voltage stability, security & control, Proceedings of the ECC/NSF workshop, Davos, Switzerland, August 1994.

[44] C.A. Canizares, Conditions for saddle-node bifurcations in AC/DC power systems, Electrical Energy & Power Systems, Vol. 17, No. 1, pp. 61-68, 1995.

[45] Y. V. Makarov, D. H. Popovic, and D.J. Hill, "Stabilization of Transient Processes in Power Systems by an Eigenvalue Shift Approach", IEEE Transactions on Power Systems, Vol. 13, Issue 2, May 1998, pp. 382 – 388.

[46] Yu. E. Gurevich, L.E. Libova, and A.A. Okin, "Design of Stability and Emergency Control Automatic Devices in Power Systems", Energoatomizdat, Moscow, 1990 – in Russian.

[47] R. R. Austria, X. Y. Chao, N. P. Reppen, and D. E. Welsh, "Integrated Approach to Transfer Limit Calculations", IEEE Computer Applications in Power, January 1995, pp. 48-52.

[48] B. Gao, G.K. Morison and P. Kundur, "Towards the Development of a Systematic Approach for Voltage Stability Assessment of Large-Scale Power Systems", IEEE Transactions on Power Systems, Vol. PWRS-11, No. 3, August 1996, pp. 1314-1324.

[49] V.A. Matveev, "A Method of Numeric Solution of Sets of Nonlinear Equations", Zhurnal Vychislitelnoi Matematiki I Matematicheskoi Fiziki, Vol. 4, No. 6, pp. 983-994, 1964 - in Russian.

[50] V.I. Tarasov, "Implementation of a Permanent Loading Procedure to Definition of Load Flows on a Limit of Aperiodic Steady-State Stability", Voprosy primeneniya matematicheskih metodov pri upravlenii regimami i razvitiem elektricheskih sistem, Irkutsk, pp. 50-56, 1975 – in Russian.

[51] A.M. Kontorovich, Y.V. Makarov and A. A. Tarakanov, "Improvements of a Permanent Loading Technique to Compute Load Flows on Stability Margin", Trudy LPI, No. 380, pp. 37-41, 1982 - in Russian.

[52] A. M. Kontorovich and Y. V. Makarov, "A permanent loading technique for fast analysis of power system stability limit load flows", USSR National Scientific and Technical Conference "Problems of Stability and Reliability of the USSR Power System", Dushanbe, 1989 – In Russian.

[53] P. Kessel and H. Glavitsch, "Estimating the voltage stability of a power system", IEEE Transactions on Power Delivery, Vol.PWRD-1, No. 3, July 1986, pp. 346-354.

[54] G. B. Price, "A generalized circle diagram approach for global analysis of transmission system performance", IEEE Trans. Power Apparatus and Systems, Vol. PAS-103, No. 10, pp. 2881–2890, October 1984, pp. 2881-2890.

[55] V. Ajjarapu and C. Christy, "The Continuation Power Flow : A Tool to Study Steady State Voltage Stability," IEEE Transactions on Power Systems, Vol. 7, No. 1, February 1992, pp. 416-423.

[56] T. Van Cutsem, C. Vournas, "Voltage Stability of Electric Power Systems", Kluwer Academic Publishers (Power Electronics and Power Systems Series), Boston, 1998

[57] A. Bihain, G. Burt, F. Casamatta, T. Koronides, R. Lopez, S. Massucco, D. Ruiz-Vega, and C. Vournas, "Advanced Perspectives and Implementation of Dynamic Security Assessment in the Open Market Environment", CIGRE 2002, France, August 2002.

[58] J. Jarjis and F.D. Galiana, "Quantitative Analysis of Steady State Stability in Power Networks", IEEE Trans. On Power Apparatus and Systems, Vol. PAS-100, No. 1, January 1981, pp. 318-326.

[59] A.M. Kontorovich, A.V. Kryukov, Y.V. Makarov, et al, Methods of stability indices computations for complicated power systems, Publishing House of the Irkutsk University, Irkutsk, 1988 (in Russian).

[60] C.A. Cañizares and F.L. Alvarado, "Computational Experience with the Point of Collapse Method on Very Large AC/DC Systems", Proceedings: Bulk Power System Voltage Phenomena - Voltage Stability And Security, ECC/NSF Workshop, Deep Creek Lake, MD, August 1991; published by ECC Inc., Fairfax, Virginia.

[61] T. Van Custem, "A method to compute reactive power margins with respect to voltage collapse", IEEE Trans. on Power Systems} Vol. 6, No. 1, February 1991, pp. 145-156.

[62] C. A. Cañizares, , F. L. Alvarado, C. L. DeMarco, I. Dobson, W. F. Long, "Point of Collapse Methods Applied to AC/DC Power Systems", IEEE Transactions on Power Systems, Vol. 7, Issue 2, May 1992, pp. 673 – 683.

[63] I. Dobson, "Observations on the Geometry of Saddle Node Bifurcation and Voltage Collapse in Electrical Power Systems", IEEE Transactions on Circuits and Systems I: Fundamental Theory and Applications, Vol. 39, Issue 3, March 1992, pp. 240 – 243.

[64] P. W. Sauer and B. C. Lesieutre, "Power System Load Modeling", J. H. Chow, P. V. Kokotovic and R. J. Thomas, (Editors), Systems and Control Theory for Power Systems, Springer-Verlag 1995, pp. 283-313.

[65] P. A. Löf, T. Smed, G. Andersson, and D. J. Hill, "Fast Calculation of a Voltage Stability Index," IEEE Trans. Power Systems, vol. 7, no. 1, pp. 54–64, February 1992.

[66] Y. Tamura, H. Mori, and S. Iwamoto, "Relationship Between Voltage Instability and Multiple Load Flow Solutions in Electric Power Systems,", IEEE Trans. on Power Apparatus and Systems, Vol.PAS-102, pp.1115 --1123, May 1983.

[67] C.J. Parker, I.F. Morrison, and D. Sutanto, "Application of an Optimization Method for Determining the Reactive Margin From Voltage Collapse in Reactive Power Planning," IEEE Trans. Power Systems, Vol. 11, No. 3, August 1996, pp. 1473–1481.

[68] G.D. Irisarri, X. Wang, J. Tong, and S. Mokhtari, "Maximum Loadability of Power Systems Using Interior Point Non-linear Optimization Method," IEEE Trans. Power Systems, Vol. 12, No. 1, February 1997, pp. 162-172.

[69] "Operations Review of June 14, 2000 PG&E Bay Area System Events Using AEMPFAST ® Software", Consultant Report P500-03-085F, Prepared by CERTS for the California Energy Commission, October 2003.

[70] I. Dobson and L. Lu, "Computing an Optimal Direction in Control Space to Avoid Saddle Node Bifurcation and Voltage Collapse in Electric Power Systems", IEEE Trans. on Automatic Control, Vol. 37, No. 10, October 1992, pp. 1616-1620.

[71] I. Dobson, L. Lu and Y. Hu, "A Direct Method for Computing a Closest Saddle Node Bifurcation in the Load Power Parameter Space of an Electric Power System", IEEE International Symposium on Circuits and Systems, Singapore, June 1991, pp. 3019-3022.

[72] I. Dobson and L. Lu, 'New Methods for Computing a Closest Saddle Node Bifurcations and Worst Case Load Power Margin for Voltage Collapse", IEEE Trans. on Power Systems, Vol. 8, No. 3, August 1993, pp. 905-913.

[73] F. Alvarado, I. Dobson and Y. Hu, "Computation of Closest Bifurcations in Power Systems", IEEE Trans. on Power Systems, Vol. 9, No. 2, May 1994, pp. 918-928.

[74] Y.V. Makarov, Q. Wu, D.J. Hill, D.H. Popovic and Z.Y. Dong, "Coordinated Steady-State Voltage Stability Assessment and Control", Proc. International Conference on Advances in Power System Control, Operation and Management APSCOM'97, Wanchai, Hong Kong, November 11-14, 1997.

[75] J. Kanetkar and S. Ranade, "Compact Representation of Power System Security - A Review," Proceedings of the North American Power Symposium, Reno, Nevada, 1992, pp. 312-321.

[76] F. D. Galiana, "Power Flow Feasibility and the Voltage Collapse Problem", Proceedings of 23rd CDC, Las Vegas, NV, December 1984, pp. 485-487.

[77] P. Kessel and H. Glavitsch, "Estimating the Voltage Stability Regions of a Power System," IEEE Transactions Power Delivery, Vol. PWRD-1, July 1986, pp. 346-354.

[78] J. D. McCalley, S. Wang, R. T. Treinen, and A. D. Papalexopoulos, "Security Boundary Visualization for Systems Operation", IEEE Transactions on Power Systems, Vol. 12, No. 2, May 1997, pp. 940-947.

[79] G. Zhou and J. D. McCalley, "Composite Security Boundary Visualization", IEEE Transactions on Power Systems, Vol. 14, No. 2, May 1999, pp. 725-731.

12/2/07 REV 6/92008

[80] J. Su, Y. Yu, H. Jia, P. Li, N. He, Z. Tang, and H. Fu, "Visualization of Voltage Stability Region of Bulk Power System", Proceedings of International Conference on Power System Technology PowerCon 2002, Vol. 3, 2002, pp. 1665-1668.

[81] M. A. Pai, "Power System Stability", Amsterdam, The Netherlands: North Holland, 1981.

[82] Y. Zeng and Y. Yu, "A Practical Direct Method for Determining Dynamic Security Regions of Electrical Power Systems", Proceedings of the International Conference on Power System Technology PowerCon 2002, Vol. 2, 2002, pp. 1270-1274.

[83] I. A. Hiskens and R. J. Davy, "Exploring the Power Flow Solution Space Boundary", IEEE Transactions on Power Systems, Vol. 16, No. 3, August 2001.

[84] Y.V. Makarov, V.A. Maslennikov, and D.J. Hill, "Calculation of Oscillatory Stability Margins in the Space of Power System Controlled Parameters", Proc. of the International Symposium on Electric Power Engineering Stockholm Power Tech, Vol. Power Systems, Stockholm, Sweden, June 1995, pp. 416-422.

[85] Y. V. Makarov and I. A. Hiskens, "A continuation method approach to finding the closest saddle node bifurcation point", Proceedings of the NSF/ECC Workshop on Bulk Power System Voltage Phenomena III, Davos, Switzerland, August 1994. Published by ECC Inc., Fairfax, Virginia.

[86] K. Huang and H. Yee, "Improved Tangent Hyperplane Method for Transient Stability Studies", Proceedings of the International Conference on Advances in Power System Control APSCOM-91, Vol. 1, 5-8 November, 1991, pp. 363 – 366.

[87] M. Djukanovic, D. J. Sobajic, and Y.-H. Pao, "Learning Tangent Hypersurfaces for Fast Assessment of Transient Stability, Proceedings of the Second International Forum on Applications of Neural Networks to Power Systems ANNPS '93, 19-22 April 1993, pp. 124 – 129.

[88] Y. Yu, Y. Zeng, C. Huang, S. T. Lee, and P. Zhang, "A Practical Direct Method for Determining Dynamic Security Regions of Electrical Power Systems by Power Perturbation Analysis", International Conference on Electrical Engineering ICEE2004, July 4-8, 2004, Sapporo, Japan.

[89] S. A. Sovalov and V. A. Semenov, Emergency Control in Power Systems, Energoatomizdat, Moscow, 1988 – in Russian.

[90] M. A. El-Sharkawi, R. J. Marks, M. E. Aggoune, D. C. Park, M. J. Damborg, and L. E. Atlas, "Dynamic Security Assessment of Power Systems Using Back Error Propagation Artificial Neuron Networks," Proceedings of the 2nd Symposium on Expert System Applications to Power Systems, Seattle, WA, July 1989.

[91] R. Kumar, A. Ipahchi, V. Brandwajan, M. A. El-Sharkawi, and G. Cauley, "Neuron Networks for Dynamic Security Assessment of Large Scale Power Systems: Requirements Overview," Proceedings of 1st International Forum on Applications of Neuron Networks to Power Systems, Seattle, WA, July 1991, pp. 65-71.

[92] A.A. EI-Keib and X. Ma, "Application of Artificial Neural Networks in Voltage Stability Assessment," IEEE Transactions on Power System, Vol. 10, No.4, Nov. 1995, pp. 1890-1896.

[93] S. Chauhan and M.P. Dava, "Kohonen Neural Network Classifier for Voltage Collapse Margin Estimation," Electric Machines and Power Systems, Vol. 25, No. 6, July 1997, pp. 607-619.

[94] Y. Mansour, A. Y. Chang, J. Tamby, E. Vaahedi, B. R. Corns, and M. A. El-Sharkawi, "Large Scale Dynamic Security Screening and Ranking Using Neuron Networks," IEEE Transactions on Power Systems, Vol. 12, No. 2, May 1997, pp. 954-960.

[95] H B Wan and Y H Song, "Hybrid Supervised and Unsupervised Neural Network Approach to Voltage Stability Analysis", Electric Power System Research, Vol. 47, No. 2, 1998, pp.115-122.

[96] V. R. Dinavahi and S. C. Srivastava, "ANN Based Voltage Stability Margin Prediction", IEEE Power Engineering Society Summer Meeting 2001, Vol. 2, 15-19 July 2001, pp. 1275-1280.

[97] A. Sittithumwat and K. Tomsovic, "Dynamic Security Margin Estimation Using Artificial Neural Networks", IEEE Power Engineering Society Summer Meeting 2002, Vol. 3, 2002, pp. 1322- 1327.

[98] M. M. Salamaa, E. M. Saieda, M. M. Abou-Elsaada, and E. F. Gharianyb, "Estimating the Voltage Collapse Proximity Indicator Using Artificial Neural Network", Energy Conversion and Management, Vol. 42, No. 1, January 2001, pp. 69-79.

[99] H. Hakim, "Application of Pattern Recognition in Transient Security Assessment," Journal of Electrical Machines and Power Systems, Vol. 20, 1992, pp. 1-15.

[100] L. Wehenkel, Automatic Learning Techniques in Power Systems, Kluwer Academic Publishers, MA, 1998.

[101] C. Aldea and S. C. Savulescu, "Evaluation of the Stability Reserve of Transelectrica's Transmission System by Using Quickstab Professional", WEC Regional Energy Forum – FOREN 2004, Neptun, 13-17 June 2004.

[102] P. Dimo, "L'Analyse Nodale des Réseaux D'Énergie", Eyrolles, 1971.

[103] T. Van Cutsem, C. Vournas, "Voltage Stability of Electric Power Systems", Kluwer Academic Publishers (Power Electronics and Power Systems Series), Boston, 1998.

[104] T. Van Cutsem and R. Mailhot, "Validation of a Fast Voltage Stability Analysis Method on the Hydro-Quebec System", IEEE Transactions on Power Systems, Vol. 12, No. 1, February 1997.

[105] F. Paganini, B.C. Lesieutre, "Generic Properties, One-Parameter Deformations, and The BCU Method", IEEE Transactions On Circuits And Systems I: Fundamental Theory And Applications", Vol. 46, No. 6, pp. 760-763, June 1999.

[106] H.-D. Chiang, C.-C. Chu, and G. Cauley, "Direct Stability Analysis of Electric Power Systems Using Energy Functions: Theory, Applications, and Perspective", Proceedings of the IEEE, 13, 1995, pp. 1497-1529.

[107] H.-D, Chiang, C.-S. Wang, and H. Li, "Development of BCU classifiers for on-line dynamic contingency screening of electric power systems", IEEE Transactions on Power Systems, 14, 1999, pp. 660-666.

[108] Y. V. Makarov, Z.-Y. Dong, and D. J. Hill, "A General Method for Small Signal Stability Analysis", IEEE Transactions on Power Systems, Vol. 13, Issue 3, August 1998, pp. 979 – 985.

[109] Z.-Y. Dong, Y.V. Makarov, and D.J. Hill, "Genetic Algorithms in Power System Small Signal Stability Analysis", Fourth International Conference on Advances in Power System Control, Operation and Management APSCOM-97, Vol. 1, November 11-14, 1997, pp. 342 - 347 (Conference Publication No. 450).

[110] A.A. Fouad and V. Vittal, Power System Transient Stability Analysis Using the Transient Energy Function Method, Prentice Hall, 1991.

[111] I. Dobson, "Computing a Closest Bifurcation Instability in Multidimensional Parameter Space", Journal of Nonlinear Science, Vol. 3, 1993, pp. 307-327.

[112] Y.V. Makarov, V. A. Maslennikov, and D. J. Hill, "Calculation of Oscillatory Stability Margins in the Space of Power System Controlled Parameters", Proc. International Symposium on Electric Power Engineering Stockholm Power Tech: Power Systems, Stockholm, Sweden, 18-22 June, 1995, pp. 416-422.

[113] Y. V. Makarov, D. J. Hill, and Z.-Y. Dong, "Computation of Bifurcation Boundaries for Power Systems: A New Δ-Plane Method", IEEE Transactions on Circuits and Systems I: Fundamental Theory and Applications, Vol. 47, Issue 4, April 2000, pp. 536 – 544.

[114] Y.V. Makarov, D. J. Hill, and I. A. Hiskens, "Properties of Quadratic Equations and Their Application to Power System Analysis", Electrical Power and Energy Systems, 22 (2000), pp. 313-323.

[115] M. Fulczyk and M. Sobierajski, "Probabilistic assessment of power system voltage stability margin using P-Q curve", Proc. 8th International Conference on Probabilistic Methods Applied to Power Systems PSCE'2004, Iowa State University, Ames, Iowa, September 2004.

[116] "Voltage Stability/Security Assessment and On-Line Control", EPRI technical report TR-101931-V1-4, Vol. 1-4, 1993.

[117] "Voltage Stability Analysis Program (VSTAB)", Version 2.1, User's Manual, EPRI Research ProjectRP30400-01, August 1992.

[118] Xiaokang Xu, M. W. Gustafson, B.P Lam, J. D. Mountford., and S. L. Johnson, "Assessment of Voltage Stability and Real and Reactive Margins Using Advanced Analytical Tools", Proceedings of International Conference on Power System Technology PowerCon 2002, Vol. 4, 2002, pp. 2047 – 2051.

[119] "VSAT – Voltage Security Assessment Tool", Available online: http://www.dsapowertools.com/downloads/VSAT_Brochure.pdf.

[120] "PowerWorld Simulator – PVQV", Available online: http://www.powerworld.com/products/pvqv.asp.

[121] S. Lockwood, R. Navarro, E. Bajrektarevic, P. Burke, S. Kang, P. Ferron, V. Kotecha, S. Kolluri, M. Nagle, S. Lee, P. Zhang, S. K. Agarwal, M. Papic, J. Useldinger, P. C. Patro, L. Arnold, D. Osborn, L. Fan, L. Hopkins, Member, M. Y. Vaiman, and M. M. Vaiman, "Utility Experience Computing Physical and Operational Margins: Part I – Basic Concept and Evaluation", 2004 IEEE PES Power Systems Conference & Exposition, New York, NY, October 10 - 13, 2004.

[122] S. Lockwood, R. Navarro, E. Bajrektarevic, P. Burke, S. Kang, P. Ferron, V. Kotecha, S. Kolluri, M. Nagle, S. Lee, P. Zhang, S. K. Agarwal, M. Papic, J. Useldinger, P. C. Patro, L. Arnold, D. Osborn, L. Fan, L. Hopkins, Member, M. Y. Vaiman, and M. M. Vaiman, "Utility Experience Computing Physical and Operational Margins: Part II – Application to Power System Studies", 2004 IEEE PES Power Systems Conference & Exposition, New York, NY, October 10 - 13, 2004.

[123] "BOR-Transient Stability: Dynamic Security Region", Available online: http://www.vrenergy.com/docs/bor-ts.pdf

[124] M. Papic, M. Y. Vaiman, and M. M. Vaiman, "Determining a Secure Region of Operation for Idaho Power Company", IEEE Power Engineering Society General Meeting, June 12-16, 2005, pp. 2720 – 2725.

[125] "NEPLAN Electricity - Voltage Stability", Available online: http://www.neplan.ch/sites/en/neplan_elec_calcmod_voltage_stability.asp.

[126] "CYMVSTAB, Voltage Stability", Available online: http://www.cyme.com/software/cymvstab/.

[127] C.D. Vournas, "Interruptible Load as a Competitor to Local Generation for Preserving Voltage Security", Available online: http://www.transmission.bpa.gov/orgs/opi/power_stability/DirLdContVournas.pdf.

[128] "On-Line Application of DSATools", Available online: http://www.dsapowertools.com/html/prod_application.php

[129] "POM - Real Time (POM-RT)", Available online: http://www.vrenergy.com/pom-rt.htm.

[130] E. Hnyilicza, S. T. Y. Lee, F. C. Scbweppe, "Steady-State Security Regions: Set-Theoretic Approach," Proceedings of the IEEE PICA Conference, pp. 347-355,1975.

[131] S. T. Lee, "Community activity room as a new tool for transmission operation and planning under a competitive power market", IEEE Bologna Power Tech Conference Proceedings, Vol. 4, 23-26 June, 2003.

[132] "QuickStab at a Glance", Available online: http://www.eciqs.com/QuickStab_at_a_Glance.htm.

[133] T. Van Cutsem, F. Capitanescu, C. Moors, D. Lefebvre, V. Sermanson, "An Advanced Tool for Preventive Voltage Security Assessment", Proc. 7th Symposium of Specialists in Electric Operational and Expansion Planning (SEPOPE), Curitiba (Brazil), May 2000.

[134] D. Ernst, D. Ruiz-Vega, M. Pavella, P. Hirsch, D. Sobajic, "A Unified Approach to Transient Stability Contingency Filtering, Ranking and Assessment", IEEE Transactions of Power Systems, Vol. 16, No. 3, August 2001.

[135] A. Bihain, G. Burt, F. Casamatta, T. Koronides, R. Lopez, S. Massucco, D. Ruiz-Vega, and C. Vournas, "Advanced Perspectives and Implementation of Dynamic Security Assessment in the Open Market Environment", CIGRE 2002, France, August 2002.

[136] T. Van Cutsem, F. Capitanescu, C. Moors, D. Lefebvre, V. Sermanson, "An Advanced Tool for Preventive Voltage Security Assessment", Proc. 7th Symposium of Specialists in Electric Operational and Expansion Planning (SEPOPE), Curitiba (Brazil), May 2000.

[137] "Local Capacity Technical Analysis", Overview of Study Report and Preliminary Results, California ISO, June 23, 2005. Available online: http://www.caiso.com/docs/2005/06/24/2005062408465116859.pdf

[138] L. Tobias, "Local Capacity Technical Analysis for Year 2006", Overview of Preliminary Results, California ISO Stakeholder Meeting, June 29, 2005. Available online: http://www.caiso.com/docs/2005/06/28/2005062816522619093.pdf

[139] "Common Information Model (CIM): CIM 10 Version", EPRI, Palo Alto, CA: 2001, 1001976. Available online: http://www.epriweb.com/public/000000000001001976.pdf

12/2/07 REV 6/92008

[140] S. Greene, I. Dobson, and F. L. Alvarado, "Sensitivity of the Loading Margin to Voltage Collapse with Respect to Arbitrary Parameters", IEEE Transactions on Power Systems, Vol. 12, Issue 1, February 1997, pp. 262 - 272

[141] S. Greene, I. Dobson, and F. L. Alvarado, "Sensitivity of Transfer Capability Margins with a Fast Formula", IEEE Transactions on Power Systems, Vol. 17, Issue 1, February 2002, pp. 34 – 40

[142] H. Wan; J. D. McCalley, V. Vittal, "Risk Based Voltage Security Assessment", IEEE Transactions on Power Systems, Vol. 15, Issue 4, Nov 2000, pp. 1247 – 1254.

[143] S. Iwamoto and Y. Tamura, "A Load Flow Calculation Method for Ill-conditioned Power Systems", Proceedings of the IEEE PES Summer Meeting, Vancouver, British Columbia, Canada, July 1979.

[144] S. Iwamoto and Y. Tamura, "A Load Flow Calculation Method for Ill-conditioned Power Systems", IEEE Trans on Power Apparatus and Systems, 1981, Vol. PAS-100(4), pp. 1736–1743.

[145] Y. V. Makarov and Z. Y. Dong , "Eigenvalues and Eigenfunctions" , Vol. 6: Computational Science and Engineering, Encyclopedia of Electrical and Electronics Engineering, edited by Professor John G. Webster, John Wiley & Sons, 1999, pp. 208-220, invited.

[146] J. H. Wilkinson, The Algebraic Eigenvalue Problem, New York: Oxford University Press, 1965.

[147] A. S. Deif, Advanced Matrix Theory for Scientists and Engineers, 2nd Edition, Abacus Press, Gordon and Breach Science Publishers, Switzerland, 1991.

[148] P.-A. Löf, G. Andersson, and D. J. Hill, "Voltage Dependent Reactive Power Limits for Voltage Stability Studies," IEEE Trans. Power Systems, Vol. 10, pp. 220-228, February 1995.

[149] P.-A. Löf, T. Smed, G. Andersson, and D. J. Hill, "Fast Calculation of a Voltage Stability Index," IEEE Trans. Power Systems, Vol. 7, pp. 54-64, February 1992.

[150] Energy Consulting International website, Available: http://www.scscc-us.com/

12/2/07 REV 6/92008